JPET Fast Forward. Published on August 4, 2021 as DOI: 10.1124/jpet.121.000695
This article has not been copyedited and formatted. The final version may differ from this version.

Title page

Bosentan alters endo- and exogenous bile salt disposition in sandwich-cultured human hepatocytes

Marlies Oorts*, Pieter Van Brantegem*, Neel Deferm, Sagnik Chatterjee, Erwin Dreesen, Axelle Cooreman, Mathieu Vinken, Lysiane Richert, Pieter Annaert

* Shared first authorship

Drug Delivery and Disposition, Department of Pharmaceutical and Pharmacological Sciences, KU Leuven, Leuven, Belgium: MO, PVB, ND, PA

Pharmaceutical Candidate Optimization, Biocon Bristol-Myers Squibb Research Center, Syngene International, Bangalore, India: SC

Clinical Pharmacology and Pharmacotherapy, Department of Pharmaceutical and Pharmacological Sciences, KU Leuven, Leuven, Belgium: ED

Uppsala Pharmacometrics Research Group, Department of Pharmacy, Uppsala University, Uppsala, Sweden: ED

Department of Pharmaceutical and Pharmacological Sciences, Vrije Universiteit Brussel, Brussels, Belgium: AC, MV

KaLy-Cell, Plobsheim, France: LR

BioNotus, Niel, Belgium: PA

JPET Fast Forward. Published on August 4, 2021 as DOI: 10.1124/jpet.121.000695
This article has not been copyedited and formatted. The final version may differ from this version.

JPET Fast Forward. Published on August 4, 2021 as DOI: 10.1124/jpet.121.000695
This article has not been copyedited and formatted. The final version may differ from this version.

Running Title page

Running title: Bosentan alters bile salt disposition

Corresponding author: Pieter Annaert, PharmD, PhD, Drug Delivery and Disposition, Department of Pharmaceutical and Pharmacological Sciences, KU Leuven, O&N2, Herestraat 49 box 921, 3000 Leuven, Belgium, tel. +32 16 33 03 03, fax. +32 16 33 07 64, Pieter.annaert@kuleuven.be

The number of text page: 43

The number of tables: 4

The number of figures: 7

The number of references: 52

The number of words in Abstract: 166

The number of words in Introduction: 699

The number of words in Discussion: 1492

Abbreviations: AUC, under the curve; BSEP, bile salt export pump; CA-d4, Cholic acid-2,2,4,4-d4; CDCA, chenodeoxycholic acid; CDF, 5-(6)- carboxy-2´,7´-dichlorofluorescein; CI, confidence interval; CWRES, conditional weighted residuals; DIC, drug-induced cholestasis;

JPET Fast Forward. Published on August 4, 2021 as DOI: 10.1124/jpet.121.000695
This article has not been copyedited and formatted. The final version may differ from this version.

DMSO, dimethyl sulfoxide; dOFV, drop in OFV; EGTA, ethylene glycol-bis(β-aminoethyl ether)-N,N,N′,N′-tetraacetic acid; ESI, electrospray ionization source; FOCE-I, first-order conditional estimation with interaction; GCA, glycocholic acid; GCDCA, glycochenodeoxycholic acid; IPRED, individual predictions; MeOH, methanol; MRP, multidrug resistance-associated protein; NTCP, sodium taurocholate co-transporting polypeptide; OATP, organic anion transporting polypeptide; OFV, objective function value; PRED, population predictions; QC, quality control; SCHH, sandwich-cultured human hepatocytes; SD, standard deviation; TCDCA, taurochenodeoxycholic acid; WEM, Williams' E Medium,

Recommended section: Toxicology

JPET Fast Forward. Published on August 4, 2021 as DOI: 10.1124/jpet.121.000695
This article has not been copyedited and formatted. The final version may differ from this version.

Abstract

Bosentan, a well-known cholestatic agent, was not identified as cholestatic at concentrations up to 200 µM based on the drug-induced cholestasis (DIC) index value, determined in a sandwich-cultured human hepatocyte (SCHH)-based DIC assay. To obtain further quantitative insights into the effects of bosentan on cellular bile salt handling by human hepatocytes, the present study determined the effect of 2.5-25 µM bosentan on endogenous bile salt levels and on the disposition of 10 µM chenodeoxycholic acid (CDCA) added to the medium in SCHH. Bosentan reduced intracellular as well as extracellular concentrations of both endogenous glycochenodeoxycholic acid (GCDCA) and glycocholic acid in a concentration-dependent manner. When exposed to 10 µM CDCA, bosentan caused a shift from canalicular efflux to sinusoidal efflux of GCDCA. CDCA levels were not affected. Our mechanistic model confirmed the inhibitory effect of bosentan on canalicular GCDCA clearance. Moreover, our results in SCHH also indicated reduced GCDCA formation. We confirmed the direct inhibitory effect of bosentan on CDCA conjugation with glycine in liver S9 fraction.

JPET Fast Forward. Published on August 4, 2021 as DOI: 10.1124/jpet.121.000695
This article has not been copyedited and formatted. The final version may differ from this version.

Significance statement

Bosentan was evaluated at therapeutically relevant concentrations (2.5-25 μM) in sandwich-cultured human hepatocytes. It altered bile salt disposition and inhibited canalicular secretion of glycochenodeoxycholate (GCDCA). Within 24 h, bosentan caused a shift from canalicular to sinusoidal efflux of GCDCA. Our results also indicated reduced GCDCA formation. We confirmed a direct effect of bosentan on chenodeoxycholic acid conjugation with glycine in liver S9 fraction.

JPET Fast Forward. Published on August 4, 2021 as DOI: 10.1124/jpet.121.000695
This article has not been copyedited and formatted. The final version may differ from this version.

1. Introduction

Pulmonary arterial hypertension is a rare and progressive disease characterized by an elevated pressure in the pulmonary arteries. Endothelin receptor antagonists such as bosentan block binding of endothelin-1 to its receptor, thereby preventing vasoconstriction (Humbert *et al.*, 2004; Gabbay *et al.*, 2007). During a European post-marketing surveillance study, it was documented that bosentan caused dose-dependent and reversible liver injury in 10.1% of the patients. For 3.2% of the patients, discontinuation of the therapy was necessary (Humbert *et al.*, 2007). Consistently, elevations in liver function markers (liver aminotransferases and bilirubin) were already shown in 16.8% of the patients during clinical studies (Fattinger *et al.*, 2001). For this reason, bosentan received a black box warning, which requires regular monitoring of the liver function markers during treatment.

Bosentan has been shown to cause cholestatic liver injury. Inhibition of bile salt transport and inhibition of bile salt secretion in particular has been attributed as one of the primary mechanisms of bosentan-induced cholestasis in several *in vitro* and *in vivo* studies (Fattinger *et al.*, 2001; Kemp *et al.*, 2005; Hartman *et al.*, 2010; Xu *et al.*, 2015). For instance, it was observed that bosentan inhibited the bile salt export pump (BSEP) function in BSEP-overexpressing membrane vesicles (Fattinger *et al.*, 2001; Mano *et al.*, 2007). Mano et al. reported that bosentan was able to inhibit human BSEP (IC_{50} = 77 µM) with comparable potency as rat BSEP (IC_{50} = 101 µM), while bosentan did not cause hepatotoxicity in rats (Fattinger *et al.*, 2001; Mano *et al.*, 2007). However, bosentan led to a stimulation of bile salt independent bile flow, rather than a reduction of the bile flow in rats (Fouassier *et al.*, 2002). These results indicate that BSEP inhibition is not the sole determinant of bosentan-induced alterations of bile salt handling. Species-specific pathways or differences in bile salt pool may alleviate the cholestatic effects of

JPET Fast Forward. Published on August 4, 2021 as DOI: 10.1124/jpet.121.000695
This article has not been copyedited and formatted. The final version may differ from this version.

bosentan due to BSEP inhibition in the rat, while this would not be the case, or to a lesser extent, in humans. Both hypotheses have been postulated by Leslie et al. who proposed an explanation for this species difference in toxicity. They demonstrated that bosentan is a more potent inhibitor of rat sodium taurocholate co-transporting polypeptide (NTCP) as compared to human NTCP (Leslie *et al.*, 2007). Moreover, next to BSEP and NTCP, bosentan can interact with several other transporters involved in bile salt homeostasis, as illustrated in Figure 1. Bosentan is both an inhibitor and a substrate of the organic anion transporting polypeptide 1B1 and 1B3 (OATP1B1/1B3) (Treiber *et al.*, 2007). In addition, bosentan was able to inhibit both multidrug resistance-associated protein (MRP) 3 and MRP4 in transporter-overexpressing membrane vesicles (Morgan *et al.*, 2013). The estimated $Kp_{u,u}$ value of 34.9 for the liver by Li et al. indicates that intracellular concentrations of bosentan are also relevant for inhibition of efflux transporters (Li *et al.*, 2018). To summarize, the interference of bosentan with bile salt homeostasis is likely not only caused by BSEP inhibition. The exact mechanisms playing a role in the effect of bosentan on bile salt handling remain poorly understood.

Previously, Rodrigues et al. demonstrated that bosentan was able to alter bile salt levels and inhibit BSEP function in human hepatoma HepaRG cell cultures. Of note, the effects observed in these *in vitro* experiments were typically obtained upon exposure to supratherapeutic bosentan concentrations (20-250 µM) (Rodrigues *et al.*, 2018). Therefore, we presently examined the influence of clinically relevant bosentan concentrations (2.5-25 µM) (Dingemanse and van Giersbergen, 2004; Nakau *et al.*, 2016; Berger *et al.*, 2017). This approach was undertaken in an attempt to reveal previously unidentified mechanisms involved in bosentan-mediated alteration of bile salt handling in SCHH. SCHH were applied as a ‘gold standard’ tool as they preserve all enzymes as well as uptake and efflux transporters responsible for the hepatic drug disposition

JPET Fast Forward. Published on August 4, 2021 as DOI: 10.1124/jpet.121.000695
This article has not been copyedited and formatted. The final version may differ from this version.

(De Bruyn *et al.*, 2013). The regulating effects of nuclear receptors, which are expected to play an important role during long-term incubations, are also maintained in sandwich-culture (Su and Waxman, 2004; Swift *et al.*, 2010; Parmentier *et al.*, 2018). Cellular pathways related to drug-induced cholestasis, such as mitochondrial toxicity and oxidative stress, have been demonstrated in sandwich-cultured hepatocytes (Yerushalmi *et al.*, 2001; Sokol *et al.*, 2005).

JPET Fast Forward. Published on August 4, 2021 as DOI: 10.1124/jpet.121.000695
This article has not been copyedited and formatted. The final version may differ from this version.

2. Materials and methods

2.1. Sandwich-cultured human hepatocytes

Cryopreserved human hepatocytes, kindly provided by KaLy-Cell, were thawed as described previously (Almeida *et al.*, 2002). See supplementary material for more details. The demographics and characteristics of the human batches used in this study are shown in Supplementary Table 1.

2.2. Hepatobiliary disposition of carboxydichlorofluorescein in SCHH

Before the start of the experiments, the biliary secretory function in SCHH was qualitatively evaluated, as described previously (Oorts *et al.*, 2016). Biliary networks were visualized by 5-(6)- carboxy-2´,7´-dichlorofluorescein (CDF) via fluorescence microscopy (excitation wavelength: 490 nm; emission wavelength: 520 nm).

2.3. Determination of endogenous bile salts in presence of bosentan in SCHH

SCHH at day 5 of culture time were incubated with either dimethyl sulfoxide (DMSO) (0.2%) in culture medium or bosentan (25 μM; 0.2% DMSO) dissolved in culture medium for 0.5, 4 or 24 h. After each incubation time, culture medium samples were taken. Then, in case of the 0.5 and 4 h time points, cells were washed twice with culture medium. Next, the cells were incubated for 23.5 and 20 h, respectively, with culture medium (supplemented with 0.2% DMSO). This recovery period was included in the incubation design in order to investigate the reversibility of the possible effects of bosentan on the endogenous bile salt disposition. After 24 h, culture

JPET Fast Forward. Published on August 4, 2021 as DOI: 10.1124/jpet.121.000695
This article has not been copyedited and formatted. The final version may differ from this version.

medium samples were again taken, after which cells were washed 3 times with cold standard buffer. Finally, cells were lysed with 250 µL of 100% methanol (MeOH) containing internal standard (200 nM CA-d4). A schematic representation of the incubation protocol is shown in Figure 2A.

2.4. Determination of CDCA disposition in presence of bosentan in SCHH

SCHH at day 5 of culture time were incubated with CDCA in presence and absence of various concentrations of bosentan to determine the influence of bosentan on the overall CDCA disposition. A schematic representation of the protocols is provided in Figure 2, including an accumulation study (Figure 2B) and an efflux study (Figure 2C).

During the accumulation study, the culture medium that was applied on the SCHH at day 4 of culture time was sampled to determine the endogenous bile salt levels in SCHH. Then, a loading phase was initiated by incubating the cells with 10 µM CDCA in presence and absence of bosentan at 2 different clinically relevant concentrations (Dingemanse and van Giersbergen, 2004; Nakau *et al.*, 2016; Berger *et al.*, 2017), i.e., 7.5 or 25 µM (1× and 3× total C_{max}, respectively; 0.2% final DMSO concentration; 250 µL/well) for different incubation times (0.5 – 1 – 4 – 12 and 24 h). A sample of culture medium from each well was taken at time 0 and after each loading time. Afterwards, cells were washed three times with 250 µL/well ice-cold standard buffer and were subsequently lysed with 250 µL of 100% MeOH containing internal standard (200 nM CA-d4) for 45 min.

During the efflux study, three different concentrations of bosentan, namely 2.5, 7.5 and 25 µM (final DMSO concentration: 0.2%) were incubated together with 10 µM CDCA for different incubation times: 0.5 – 1 – 4 – 12 and 24 h. A culture medium sample of each well was taken at

JPET Fast Forward. Published on August 4, 2021 as DOI: 10.1124/jpet.121.000695
This article has not been copyedited and formatted. The final version may differ from this version.

time 0 and after each loading time, another culture medium sample was collected. Afterwards, the cells were washed two times with either ice-cold standard buffer or ice-cold Ca^{2+}/Mg^{2+}-free buffer ($Ca^{2+/}Mg^{2+}$-free Hanks' balanced salt solution containing 1 mM EGTA, 10 mM HEPES and adjusted to pH 7.4) (250 µL/well). Subsequently, the SCHH were incubated with pre-warmed either standard or Ca^{2+}/Mg^{2+}-free buffer for 15 min. The amounts of CDCA and its conjugates taurochenodeoxycholic acid (TCDCA) and GCDCA found in the standard buffer represent the amounts that were effluxed across the sinusoidal membrane. The amounts of bile salts found in the Ca^{2+}/Mg^{2+}-free buffer represent the amounts of bile salts effluxed across both the sinusoidal and canalicular membrane. Depletion of Ca^{2+} and Mg^{2+} in the extracellular medium will result in opening of tight junctions leading to the release of canalicular contents into the buffer (Liu *et al.*, 1999). After 15 min, buffer samples in each well were collected and cells were rinsed three times with ice-cold standard buffer. Finally, cells were lysed with 250 µL of 100% MeOH containing internal standard (200 nM CA-d4) for 45 min. Medium samples taken at time 0 were diluted with 4 volumes of 100% MeOH containing internal standard (200 nM CA-d4), while all other medium and buffer samples were diluted with 1 volume of 100% MeOH containing internal standard. All samples were stored at -20°C prior to the day of analysis.

2.5. Glycine conjugation of CDCA in human liver S9 fraction

The conjugation reaction was performed as described previously (Thakare *et al.*, 2018). In brief, the liver S9 fractions was incubated at a final concentration of 1 mg protein/mL in 100 mM potassium phosphate buffer containing 5 mM $MgCl_2$ at pH 7.4. After preincubated for 10 min at 37°C with 10 µM or 50 µM CDCA in the presence and absence of 25 µM, 85 µM and 250 µM bosentan, the prewarmed cofactor mixture was added to initiate the reaction. The cofactor

JPET Fast Forward. Published on August 4, 2021 as DOI: 10.1124/jpet.121.000695
This article has not been copyedited and formatted. The final version may differ from this version.

mixture of consisted of 5 mM taurine, 5 mM glycine, 0.4 mM coenzyme A, 1 mM MgATP, 1 mM NADPH and 3 mM glucose-6-phospate (final concentrations). The reaction mixture was incubated at 37°C for 60 min. Subsequently, the reaction was quenched by adding 100 µL of the reaction mixture to 100 µL of ice-cold MeOH and vortexing. Samples were stored at -80°C until analysis.

2.6. Sample preparation for determination of bile salts

Samples taken from the culture medium at time 0 were further diluted with one volume of MeOH containing internal standard, while all other samples were processed undiluted. Next, medium, buffer and lysate samples were centrifuged at 20,816 × *g* for 15 min at 4°C. Then, samples were evaporated until dryness using a rotary vacuum evaporator (Martin Christ Gefriertrocknungsanlagen GmbH, Osterode am Harz, Germany) and reconstituted in a mixture of 50:50 MeOH:ammonium acetate buffer with acetic acid (5 mM; adjusted to pH 3.5). Samples were vortexed for 1 min and stored at -20°C. At the day of analysis, samples were centrifuged again at 20,816 × *g* for 15 min at 4°C and transferred into micro-inserts for LC-MS/MS analysis.

2.7. Bioanalysis of bile salts

Bile salt analysis was performed with a Accela™ U-HPLC system (Thermo Fisher, Breda, The Netherlands) coupled to a TSQ Quantum Access™ triple quadrupole mass spectrometer, equipped with an electrospray ionization source (ESI). Data acquisition and peak integration were performed with the XcaliburR 2.0.7 and LCquanR 2.5.6 Software Packages, respectively. A Kinetex XB-C18 column (2.6 µm, 100 Å, 50 mm x 2.1 mm) with an in-line KrudKatcher ultra

JPET Fast Forward. Published on August 4, 2021 as DOI: 10.1124/jpet.121.000695
This article has not been copyedited and formatted. The final version may differ from this version.

HPLC filter (Phenomenex, Utrecht, The Netherlands) was used for optimal separation. The total run time was 12 min and the injection volume 25 µL (full loop mode). The column oven and sample tray temperatures were set at 30°C and 15°C, respectively. The flow rate was 450 µL/min. The bile salts were eluted using a gradient (Supplementary Table 2).

Analysis was performed using negative ESI mode with following parameters: capillary temperature 275°C, vaporizer temperature 300°C, sheath gas (N_2) pressure 40 (arbitrary units), auxiliary gas (N_2) pressure 45 (arbitrary units), ion sweep pressure 20 (arbitrary units), spray voltage 3,500 V, and collision gas (Ar) 1.5 mTorr. Parent and daughter m/z ratios together with collision energies are shown in Supplementary Table 3. Three groups of bile salts show identical masses and daughter ions, for which they were separated using LC. Quality control (QC) concentrations were 50, 500 and 2,000 nM. Intra- and interday precision of these QC samples were below 15% for the high and middle high concentration and below 20% for the low concentration. The calibration curves were linear in a range between 9.8 and 5,000 nM.

2.8. Data analysis

During the efflux study, cells were either incubated with standard buffer to determine sinusoidal efflux only, or with Ca^{2+}/Mg^{2+}-free buffer to determine sinusoidal and canalicular efflux simultaneously ('total efflux'). Canalicular efflux was calculated by subtracting the amount of bile salts obtained in standard buffer from amount of bile salts obtained in Ca^{2+}/Mg^{2+}-free buffer. After the efflux phase, the cells were lysed. Lysates of cells that had been treated with standard buffer represent the residual amounts in the cells+canaliculi, while lysates of cells treated with Ca^{2+}/Mg^{2+}-free buffer represent the residual amounts in cells only.

JPET Fast Forward. Published on August 4, 2021 as DOI: 10.1124/jpet.121.000695
This article has not been copyedited and formatted. The final version may differ from this version.

The intracellular concentration after loading was calculated by taking the sum of the amount of bile salts in standard buffer after efflux (i.e., the sinusoidal efflux) and the lysates from the conditions that were treated with Ca^{2+}/Mg^{2+}-free buffer after efflux (cells only). Intracellular bile salt concentrations were calculated based on the ratio of the intracellular amounts of bile salts and the total hepatocyte volume of 1.37 µL per 200,000 cells. This volume was based on the mean value of 6.85 pL/cell for human hepatocytes (Matsui *et al.*, 1996; Morales-Navarrete *et al.*, 2015). A total of 250,000 cells were seeded per well, while an 80% attachment rate was assumed.

The sinusoidal efflux clearance (nL/min) was calculated according to the following equation:

$$\text{Sinusoidal efflux clearance} = \frac{\text{Amount in standard buffer}}{\text{AUC}_{\text{intracellular}}}$$

Equation 1.

In addition, the canalicular efflux clearance (nL/min) was calculated based on equation 2.

$$\text{Canalicular efflux clearance} = \frac{\text{Amount in } Ca^{2+}/Mg^{2+}\text{-free buffer} - \text{Amount in standard buffer}}{\text{AUC}_{\text{intracellular}}}$$

Equation 2.

For both equations, the area under the curve (AUC) value was calculated using the PKNCA package in R version 3.6.2. The $AUC_{intracellular}$ was calculated from the mean decrease in intracellular bile salts during an efflux phase of 15 min, initiated after each loading phase.

To elucidate differences between disposition profiles of CDCA and its conjugate GCDCA in the absence or presence of bosentan, mean AUC (± SD) values were calculated, using the PKNCA

JPET Fast Forward. Published on August 4, 2021 as DOI: 10.1124/jpet.121.000695
This article has not been copyedited and formatted. The final version may differ from this version.

package in R version 3.6.2. To test whether the AUCs differed statistically significantly from the control, a Dunnett's test was applied. In addition, this statistical test was also used to compare the conditions with bosentan and control conditions. A two-tailed unpaired t-test was applied to evaluate difference between two groups. P values were considered to be statistically significant when $p < 0.05$.

2.9. Mechanistic modeling of bile salt disposition

Mechanistic modeling was performed in NONMEM version 7.4 (ICON Development Solutions, Gaithersburg, MD, USA) using first-order conditional estimation with interaction (FOCE-I) to estimate the parameters. ADVAN13 was selected as differential equation solver. The structural model was based on the experimental design and previously established models (Figure 3A) (Pfeifer *et al.*, 2013; Yang *et al.*, 2015; Guo *et al.*, 2016; Keemink *et al.*, 2018). The amount of CDCA administered to compartment 1 was calculated based on the mean measured amount of CDCA in the culture medium at time 0 for all conditions. Since the amounts of CDCA in the canaliculi were negligible at all time points and almost no CDCA is found in human bile (Matsson *et al.*, 2009), no biliary compartment of CDCA was included in the structural model. V_{med} defined as the incubation volume (250 µL). V_{cell} was fixed to 1.37 µL based on the mean of two literature values (Matsui *et al.*, 1996; Morales-Navarrete *et al.*, 2015). Only unbound intracellular concentrations of CDCA and GCDCA ($fu_{cell,CDCA}$ and $fu_{cell,GCDCA}$, respectively) were considered to be available for clearance processes. K_{flux} represents the first order rate constant for the release of canalicular contents due to periodical canalicular contractions (Guo *et al.*, 2016). The parameters were estimated in a stepwise approach. First, CDCA uptake and clearance were explored in the absence of bosentan with GCDCA amounts in all compartments combined

JPET Fast Forward. Published on August 4, 2021 as DOI: 10.1124/jpet.121.000695
This article has not been copyedited and formatted. The final version may differ from this version.

(Supplementary Figure 1A). Linear as well as Michaelis-Menten kinetics were evaluated. Second, the GCDCA disposition was investigated with CDCA parameters fixed to the values obtained in the previous step (Supplementary Figure 1B). Finally, all parameters were estimated simultaneously and bosentan was examined as a categorical covariate on the biliary clearance of GCDCA ($CL_{bile,GCDCA}$), the efflux clearance of GCDCA ($CL_{eff,GCDCA}$) and the metabolic clearance of CDCA ($CL_{met,CDCA}$). Models were evaluated based on drop in the objective function value (OFV) (α = 0.05) and following diagnostic plots: observations versus population predictions (PRED), conditional weighted residuals (CWRES) versus PRED and CWRES versus time. All error was included as residual variability. Several residual error models were tested of which three were retained. Because the amounts in compartments 3 and 4 were calculated based on independent measurements, multiple imputation was performed with 5,000 out of 3.43×10^{143} possible combinations using the bootstrap function of PsN. This allowed evaluation of the robustness of the parameter estimates. In addition, the error model with the most successful runs was considered the best model. The median parameter estimates of the best model were used to simulate the amount of CDCA and GCDCA in each compartment for 10,000 *in vitro* experiments per bosentan concentration. The AUC in each compartment was computed based on these simulations using the PKNCA package in R version 3.6.2.

JPET Fast Forward. Published on August 4, 2021 as DOI: 10.1124/jpet.121.000695
This article has not been copyedited and formatted. The final version may differ from this version.

3. Results

3.1. The influence of bosentan on endogenous bile salts in SCHH

3.1.1. Endogenous bile salts in SCHH at day 5 of culture time

Endogenous bile salts were detected in the culture medium of SCHH at day 5 of culture time. The culture medium was replaced daily (every 24 h). Bile salts that were measured in the medium were thus newly synthesized or already present inside the cells and effluxed during the 24 h time window. GCDCA and GCA were the main bile salts present in the culture medium. Others could not be detected (Supplementary Table 3). Supplementary Figure 2 shows the concentration of both bile salts in the culture medium. GCA levels were 11.6-fold higher than GCDCA levels.

3.1.2. The influence of bosentan on endogenous bile salts in the culture medium of SCHH

The amount of GCDCA in the culture medium significantly increased with 40.4%, 45.5% and 43.4% as compared to the control when SCHH were incubated with 25 µM bosentan for 0.5, 4 h and 24 h, respectively (Figure 4A). Bosentan increased the amount of GCA with 20.3% and 10.4% as compared to the control in the culture medium after a 0.5 h and 4 h incubation, respectively , while a significant decrease of GCA accumulation (33.7%) was observed after 24 h (Figure 4B). Following incubation times of 0.5 and 4 h, culture medium without bosentan was added to evaluate whether the cells would be able to (partially) recover from the effects of bosentan on bile salt disposition. As shown in Figure 4C and Figure 4D, the relative amounts of GCDCA and GCA were similar to the controls (no bosentan exposure) after a 0.5 h treatment of

JPET Fast Forward. Published on August 4, 2021 as DOI: 10.1124/jpet.121.000695
This article has not been copyedited and formatted. The final version may differ from this version.

bosentan followed by a 23.5 h recovery period, while GCA decreased with 16.9% after a 4 h treatment of bosentan followed by a recovery of 20 h, when compared to the control condition.

3.1.3. The influence of bosentan on the intracellular endogenous bile salts in SCHH

Figure 4E and F show that bosentan did not alter the intracellular accumulation of GCDCA and GCA after a 0.5 h treatment, followed by a recovery period of 23.5 h. The intracellular accumulation of both bile salts was significantly decreased in the SCHH treated with bosentan for 4 h followed by a recovery period of 20 h and after 24 h treatment with bosentan. The reductions after 4 h followed by a recovery period of 20 h amounted to 22.3% and 24.2% for GCDCA and GCA, respectively. After 24 h, the presence of bosentan resulted in a 73.5% and 86.9% reduction in accumulated levels of GCDCA and GCA, respectively.

3.2. The influence of bosentan on CDCA disposition in day 5 SCHH

3.2.1. The influence of bosentan on CDCA disposition was first assessed over 24 h by quantifying CDCA and GCDCA in medium and cultures in function of time

The mean amount (± SD) of CDCA measured in the culture medium of all conditions at time 0 (immediately after addition of the dosing solution with nominal concentration of 10 µM) comprised 2,574 ± 296 pmol (equal to 10.3 ± 1.2 µM). This concentration of CDCA was chosen, based on our previous investigations on the toxicity of CDCA in SCHH by measuring the capacity of the hepatocytes to produce urea. Indeed, in exposed SCHH, CDCA caused no decrease in urea production up to 200 µM. During the incubation with CDCA, hepatocytes are able to support glycine or taurine conjugation. Consistent with earlier findings (Marion *et al.*, 2012), only GCDCA, but not TCDCA, was detected in SCHH exposed to CDCA.

JPET Fast Forward. Published on August 4, 2021 as DOI: 10.1124/jpet.121.000695
This article has not been copyedited and formatted. The final version may differ from this version.

The disappearance profiles for CDCA in the medium are shown in Supplementary Figure 3, suggesting saturable uptake. The corresponding AUCs of CDCA are depicted in Supplementary Table 4. The presence of bosentan (2.5-25 μM) did not affect the CDCA disappearance profile and corresponding AUCs. After 24 h, CDCA was no longer detected in the culture medium. Within 24 h, the hepatocytes conjugated virtually all CDCA to GCDCA, followed by the efflux of GCDCA back into the medium. A time-dependent increase in the amount of GCDCA in the culture medium was observed in all conditions tested.

The accumulated amounts after loading the cells with CDCA comprises the total amount in both cells and canaliculi (Figure 5). A time-dependent decrease in CDCA levels was observed, while the accumulated GCDCA levels initially increased, reaching steady state after 4 h of incubation time. After 24 h, accumulated levels of CDCA were below the quantification limit. Bosentan (7.5-25 μM) appeared to decrease steady-state levels of GCDCA from 12 h onwards, resulting in a significantly reduced AUC as compared to the control (Figure 5B and Table 1).

3.2.2. The influence of bosentan on in vitro biliary secretion of GCDCA based on an efflux incubation design

After exposure of SCCH for predetermined incubation times, 15 min efflux experiments with standard and Ca^{2+}/Mg^{2+}-free buffers in parallel were conducted to indirectly determine secretion to canalicular compartments. For CDCA very limited secretion was observed due to extensive intracellular metabolism (Supplementary Figure 4). The corresponding AUC values for CDCA efflux indicated that bosentan did not influence the CDCA efflux in function of time (data not shown). GCDCA showed comparable efflux rates across the sinusoidal and canalicular membranes (control conditions; Figure 6A). Importantly, in the presence of bosentan, GCDCA

JPET Fast Forward. Published on August 4, 2021 as DOI: 10.1124/jpet.121.000695
This article has not been copyedited and formatted. The final version may differ from this version.

efflux rates gradually decreased. This was also reflected by significantly decreased AUC values as compared to the control condition (Table 2).

Bosentan was able to reduce the residual intracellular amounts of GCDCA after loading followed by an efflux phase of 15 min (Supplementary Figure 5). Over time, the amount of GCDCA in the cells and cells+canaliculi increased linearly up to 4 h of incubation. After 4 h, a decrease of GCDCA was observed, suggesting secretion of GCDCA. This decrease was less pronounced in the cells+canaliculi as compared to cells only, implying that GCDCA is effluxed both across the sinusoidal and canalicular membranes. The bosentan-induced alterations of the accumulated amounts of GCDCA in cells or cells+canaliculi in function of time are also reflected by decreases in the corresponding AUC values as the bosentan concentration increases (Supplementary Table 5). The residual intracellular amounts of CDCA were not altered by bosentan (Supplementary Figure 6).

3.2.3. The influence of bosentan on the sinusoidal and canalicular efflux clearances of CDCA and GCDCA in SCHH

The sinusoidal and canalicular efflux clearances for GCDCA are represented in Figure 6E and F. A time dependent increase in sinusoidal efflux clearance was observed in the control conditions. Bosentan did not affect the clearance up to 12 h. After 24 h, the presence of bosentan increased the sinusoidal efflux clearance of GCDCA (Figure 6E). Similarly, a time-dependent increase in canalicular efflux clearance was observed in the control conditions (Figure 6F). In presence of bosentan, the canalicular efflux clearance was decreased after 24 h, suggesting that bosentan was able to inhibit the canalicular efflux pathways of GCDCA (e.g., via BSEP).

JPET Fast Forward. Published on August 4, 2021 as DOI: 10.1124/jpet.121.000695
This article has not been copyedited and formatted. The final version may differ from this version.

3.3. Determination of *fu*

Unbound fractions of CDCA and GCDCA in presence of human hepatocytes were determined using equilibrium dialysis. Values for $fu_{cell,CDCA}$ and $fu_{cell,GCDCA}$ were 0.654 ± 0.073 and 0.805 ± 0.280, respectively.

3.4. Mechanistic modeling for further elucidation of the effects of bosentan on CDCA and GCDCA hepatobiliary disposition in SCHH

The structural model developed for CDCA and GCDCA disposition in SCHH is shown in Figure 3A. Saturable uptake and linear metabolism were implemented for CDCA. All GCDCA related clearances were linear. Covariate testing showed that the effect of bosentan exposure was the most pronounced on $CL_{bile,GCDCA}$ by means of a drop in OFV (Table 3). In addition, the individual predictions showed better agreement with the observed values. The diagnostic plots of the final model do not show a clear trend although there is some deviation in the CWRES versus PRED and CWRES versus time plots (Supplementary Figure 7). The predicted amounts are in good agreement with the observed values (Supplementary Figure 8). Inclusion of bosentan as a covariate on $CL_{eff,GCDCA}$ especially improved the predictions in compartment 4. The amounts in compartment 2 (cellular amount of CDCA) were not completely captured. Incorporation of additional parameters, e.g., an extra clearance parameter for CDCA (linear and non-linear), did not result in improved predictions of intracellular CDCA amounts.

The design of the experiments necessitated the performance of prior calculations to determine the amounts in compartments 3 and 4. For initial model development, the values were subtracted from each other based on the replicate number. Because these values were obtained from

JPET Fast Forward. Published on August 4, 2021 as DOI: 10.1124/jpet.121.000695
This article has not been copyedited and formatted. The final version may differ from this version.

different wells, a multiple imputation sensitivity analysis was performed in the final model. We selected the best error model based on the most successful runs and used the resulting median parameter estimates for simulations. The best model resulted in 4,495/5,000 (89.9%) successful minimizations. In this model, residual variability was implemented as combined proportional error for compartments 1 and 5, combined proportional error for compartments 2 and 3, and additive error for both compartments 2 and 4 separately. Median parameter estimates and residual error with 95% confidence interval (CI) are represented in Table 4. The simulated amounts of CDCA or GCDCA in each compartment are depicted in Figure 3B.

The parameter estimates show that bosentan significantly alters the biliary clearance of GCDCA. The simulated intracellular CDCA and GCDCA amounts over time (compartments 2 and 3, respectively) are quasi unaltered by increasing bosentan concentrations.

3.5. Bosentan inhibits glycine conjugation of CDCA in liver S9 fraction

Because bosentan reduced intracellular GCDCA amounts of both endogenous and exogenous bile salts, we further investigated the effect of bosentan on glycine conjugation of CDCA in liver S9 fraction. The previously reported liver $Kp_{u,u}$ value for bosentan of about 35 illustrates significant accumulation of bosentan in hepatocytes relative to plasma (Li *et al.*, 2018). Based on this, bosentan concentrations of 25 µM (3 $\times$ total Cmax), 85 µM and 250 µM were selected for the *in vitro* incubations with liver S9 fraction. Bosentan at 85 µM and 250 µM significantly reduced glycine conjugation with respect to the control when incubated with both 10 µM and 50 µM CDCA (Figure 7).

JPET Fast Forward. Published on August 4, 2021 as DOI: 10.1124/jpet.121.000695
This article has not been copyedited and formatted. The final version may differ from this version.

JPET Fast Forward. Published on August 4, 2021 as DOI: 10.1124/jpet.121.000695
This article has not been copyedited and formatted. The final version may differ from this version.

4. Discussion

We previously introduced a holistic *in vitro* screening assay to investigate the cholestatic propensity of a given compound. In this assay, bosentan was not identified as cholestatic at concentrations up to 200 µM (Chatterjee, Richert, *et al.*, 2014; Oorts *et al.*, 2016; Van Brantegem *et al.*, 2020). In order to explain this result, the present study aimed to explore the mechanisms governing the bosentan-induced disturbance in bile salt homeostasis in SCHH. Bile salt disposition profiling in SCHH was considered to be highly valuable. Measuring intra- and extracellular bile salt levels could provide an earlier and more sensitive marker for a DIC signature.

The anticipated effects of bosentan (25 µM) on bile salt homeostasis were first evaluated by profiling endogenous bile salts in SCHH. Bosentan caused substantial alterations of the *in vitro* hepatic disposition of endogenous GCDCA and GCA. These findings are consistent with a mechanistic hypothesis of bosentan-mediated inhibition of formation of glycine conjugates, along with inhibition of transporter-mediated re-uptake of glycine-conjugated bile salts. This re-uptake inhibition is in accordance with the early masking of overall inhibition of bile salt synthesis. As illustrated in Figure 1, both OATP and NTCP are known to mediate bile salt uptake and both transporters are inhibited by bosentan (Hartman *et al.*, 2010; Lepist *et al.*, 2014). In addition, inhibition of biliary secretion of GCDCA and GCA by bosentan may also explain the effect on medium levels at later time points. Indeed, bile canaliculi in SCHH are known to contract with certain intervals, thereby releasing intracanalicular contents in the medium (Oshio and Phillips, 1981; Phillips *et al.*, 1982). Bile salts that are already present in these canaliculi may increase medium levels in the first hours after start of the incubation. However, at later time points these canaliculi will also be depleted of GCA and GCDCA, contributing to decreased

JPET Fast Forward. Published on August 4, 2021 as DOI: 10.1124/jpet.121.000695
This article has not been copyedited and formatted. The final version may differ from this version.

medium levels. Another mechanism possibly explaining the increased medium levels, is a shift from canalicular to sinusoidal clearance of bile salts. Based on the results for endogenous bile salts, we hypothesized that bosentan inhibits both *de novo* synthesis of bile salts and the conjugation of unconjugated bile salts. In this case, the cells were not able to fully re-establish the bile salt levels during the recovery phase due to the potentially inhibited synthesis or conjugation. Overall, these findings are in accordance with Lepist et al. who showed that bosentan at concentrations of 10 and 100 μM were able to decrease the amount of GCA and GCDCA in the cells, while only in case of GCA a decrease was seen in the culture medium after 24 h (Lepist *et al.*, 2014).

In a second phase of this research, we challenged the SCHH with an intermediate, yet non-cytotoxic concentration of exogenously added CDCA (10 μM) to evaluate the bile salt processing capacity of the hepatocytes in presence of different bosentan concentrations (2.5-25 μM). CDCA and its metabolite GCDCA have been used as prototypic bile salts of interest for the following reasons. (1) The levels of both bile salts comprise more than 40% of the total serum bile salt pool in human plasma (Gnewuch *et al.*, 2009; Scherer *et al.*, 2009; Xiang *et al.*, 2010). (2) Both bile salts play an important role in the onset of bile salt induced toxicity, eventually leading to cholestasis (Lepist *et al.*, 2014). (3) Finally, hepatocytes have the capability to convert CDCA to GCDCA. Another strength of the present experimental design over previously performed studies is the use of clinically relevant bosentan concentrations, i.e., 2.5 μM, 7.5 μM and 25 μM, in a protein-containing medium (Dingemanse and van Giersbergen, 2004; Dawson *et al.*, 2012). In contrast, most previously conducted *in vitro* studies showed the effects of bosentan using very high concentrations up to 300 μM (Rodrigues *et al.*, 2018).

JPET Fast Forward. Published on August 4, 2021 as DOI: 10.1124/jpet.121.000695
This article has not been copyedited and formatted. The final version may differ from this version.

Sinusoidal efflux of bile salts becomes more important with increasing levels of bile salts in the blood (or in the culture medium *in vitro*) as a result (Soroka *et al.*, 2001; Boyer *et al.*, 2006; Chatterjee, Bijsmans, *et al.*, 2014). In addition, bosentan was expected to block re-uptake of conjugated bile salts by inhibition of NTCP and OATP1B1 and 1B3 (Leslie *et al.*, 2007; Treiber *et al.*, 2007). However, the unaltered levels of CDCA and GCDCA in the medium contradict this (Supplementary Figure 3). Augmented intracellular bosentan concentrations as compared to the concentrations in the medium might contribute to this effect. Recently, it has been predicted that the *in vitro* $Kp_{u,u}$ value of bosentan is 34.9 (95% CI 4.2-50) (Li *et al.*, 2018), resulting in an accumulation of bosentan in the liver, depletion in the medium, and the reduced ability to inhibit uptake transporters. Moreover, bosentan is also extensively metabolized by CYP2C9 and CYP3A4 and the role of its metabolites has not been fully elucidated yet (Markova *et al.*, 2013).

The significant effect of bosentan as covariate on $CL_{bile,GCDCA}$ in the final model is consistent with the current hypothesis that BSEP inhibition plays a role in bosentan-induced cholestasis. Bosentan is a known BSEP inhibitor with a reported IC_{50} value of 42.1 µM (Lepist *et al.*, 2014). Paradoxically, we observed a reduced intracellular GCDCA accumulation. However, we confirmed the inhibitory effect of bosentan on glycine conjugation of CDCA, which at least partially explains this observation. Reduced glycine conjugation of CDCA (and DCA) has also been observed for other cholestatic agents such as troglitazone (Ogimura *et al.*, 2017). The apparent absence of an effect on the intracellular CDCA accumulation could be caused by a reduced CDCA synthesis as a result of inhibition of the conversion of CDCA to GCDCA. Initial short-term increased CDCA levels might have activated a feed-back mechanism preventing *de novo* CDCA synthesis.

JPET Fast Forward. Published on August 4, 2021 as DOI: 10.1124/jpet.121.000695
This article has not been copyedited and formatted. The final version may differ from this version.

Adding bosentan as a covariate on the sinusoidal efflux clearance ($CL_{eff,GCDCA}$) did not result in a significant drop in OFV when additionally added to the model with bosentan as covariate on $CL_{bile,GCDCA}$. Nevertheless, we expect increased sinusoidal efflux to be an important compensatory mechanism for DIC. In addition, the effect of bosentan on metabolic clearance of CDCA ($CL_{met,CDCA}$) was not significant. The relatively large variability of the data in compartments 3 and 4 (Figure 3B) might contribute to the absence of this effect, potentially masking alterations of $CL_{met,CDCA}$ induced by bosentan. A clear trend towards lower intracellular GCDCA levels (compartment 3) can be observed as is also evident from Supplementary Figure 5. In line with the unaltered CDCA and GCDCA levels in the medium (Supplementary Figure 3), the simulations did not show an effect of bosentan on CDCA uptake. Nevertheless, the concentrations of CDCA in compartment 1 (medium) for all bosentan concentrations are slightly overpredicted which might indicate initial inhibition of CDCA uptake by bosentan. The model provided insight in the concentration-dependent effect of bosentan on the disposition of CDCA and GCDCA. Subsequent implementation in a physiologically-based pharmacokinetic model will enable studying the effect of bosentan on bile salt disposition in a mathematically more complex but mechanistically more relevant system. This will shed more light on the bile salt alterations in an *in vivo* environment in which also enterohepatic circulation of bile salts takes place. Ultimately, this might lead to the identification of a novel biomarker for DIC.

It must be noted that we explored the effect of bosentan on the disposition of a single bile salt. Nevertheless, *in vivo*, a complex bile salt pool (and not a single bile salt) serves to maintain a healthy environment for the hepatocytes (Woolbright and Jaeschke, 2015). The effects of a drug on bile salt homeostasis cannot solely be attributed to a single bile salt and this should be considered when interpreting the current results. The metabolites of bosentan might also have an

JPET Fast Forward. Published on August 4, 2021 as DOI: 10.1124/jpet.121.000695
This article has not been copyedited and formatted. The final version may differ from this version.

effect. For instance, Fattinger and colleagues have shown that the metabolite Ro 47-8634 (O-demethylation of the phenolic methyl ether of bosentan by CYP3A4) appeared to inhibit BSEP more potently than its parent (Fattinger *et al.,* 2001). Whether other metabolites are also responsible for the disturbance of bile salt homeostasis and to what extent could serve as an interesting hypothesis for further studies. In addition, it would be extremely valuable to evaluate other endothelin receptor antagonists, like macitentan, sitaxentan and ambrisentan for their ability to disturb bile salt homeostasis *in vitro*. This may support further validation of this *in vitro* assay in terms of predicting a cholestatic risk *in vivo*.

In conclusion, the current data provided unique insight into the overall interference of clinically relevant bosentan concentrations with bile salt disposition in SCHH. Bosentan altered both the endo- and exogenous bile salt handling. Mechanistic modeling revealed inhibition of the biliary clearance of GCDCA as predominant mechanism. Moreover, our data also indicated reduced GCDCA formation. We confirmed that this resulted from a direct effect of bosentan on CDCA conjugation with glycine. The reduction in biliary GCDCA output seemed to result in an initial shift towards sinusoidal efflux but also in reduced GCDCA formation. Additional factors that may play a role in the mechanisms of cholestasis caused by bosentan are the involvement of the metabolites of bosentan.

JPET Fast Forward. Published on August 4, 2021 as DOI: 10.1124/jpet.121.000695
This article has not been copyedited and formatted. The final version may differ from this version.

Authorship contributions

Participated in research design: all authors

Conducted experiments: MO, ND, PVB

Performed data analysis: MO, PA, PVB

Wrote or contributed to the writing of the manuscript: all authors

Approved the content and submission of the paper: all authors

No author has an actual or perceived conflict of interest with the contents of this article.

JPET Fast Forward. Published on August 4, 2021 as DOI: 10.1124/jpet.121.000695
This article has not been copyedited and formatted. The final version may differ from this version.

References

Almeida AM, Castel-Branco MM, and Falcão AC (2002) Linear regression for calibration lines revisited: Weighting schemes for bioanalytical methods. *J Chromatogr B Anal Technol Biomed Life Sci* **774**:215–222.

Berger RMF, Gehin M, Beghetti M, Ivy D, Kusic-Pajic A, Cornelisse P, Grill S, Bonnet D, and FUTURE-3 investigators (2017) A bosentan pharmacokinetic study to investigate dosing regimens in paediatric patients with pulmonary arterial hypertension: FUTURE-3. *Br J Clin Pharmacol* **83**:1734–1744.

Boyer JL, Trauner M, Mennone A, Soroka CJ, Cai S-Y, Moustafa T, Zollner G, Lee JY, and Ballatori N (2006) Upregulation of a basolateral FXR-dependent bile acid efflux transporter OSTalpha-OSTbeta in cholestasis in humans and rodents. *Am J Physiol Gastrointest Liver Physiol* **290**:G1124-30.

Chatterjee S, Bijsmans ITGW, van Mil SWC, Augustijns P, and Annaert P (2014) Toxicity and intracellular accumulation of bile acids in sandwich-cultured rat hepatocytes: role of glycine conjugates. *Toxicol In Vitro* **28**:218–30, Elsevier Ltd.

Chatterjee S, Richert L, Augustijns P, and Annaert P (2014) Hepatocyte-based in vitro model for assessment of drug-induced cholestasis. *Toxicol Appl Pharmacol* **274**:124–36.

Dawson S, Stahl S, Paul N, Barber J, and Kenna JG (2012) In vitro inhibition of the bile salt export pump correlates with risk of cholestatic drug-induced liver injury in humans. *Drug Metab Dispos* **40**:130–8.

De Bruyn T, Chatterjee S, Fattah S, Keemink J, Nicolaï J, Augustijns P, and Annaert P (2013) Sandwich-cultured hepatocytes: utility for in vitro exploration of hepatobiliary drug disposition and drug-induced hepatotoxicity. *Expert Opin Drug Metab Toxicol* **9**:589–616.

Dingemanse J, and van Giersbergen PLM (2004) Clinical pharmacology of bosentan, a dual endothelin receptor antagonist. *Clin Pharmacokinet* **43**:1089–115.

Fattinger K, Funk C, Pantze M, Weber C, Reichen J, Stieger B, and Meier PJ (2001) The endothelin antagonist bosentan inhibits the canalicular bile salt export pump: a potential mechanism for hepatic adverse reactions. *Clin Pharmacol Ther* **69**:223–31.

Fouassier L, Kinnman N, Lefèvre G, Lasnier E, Rey C, Poupon R, Elferink RPJO, and Housset C (2002) Contribution of mrp2 in alterations of canalicular bile formation by the endothelin antagonist bosentan. *J Hepatol* **37**:184–91.

Gabbay E, Fraser J, and McNeil K (2007) Review of bosentan in the management of pulmonary arterial hypertension. *Vasc Health Risk Manag* **3**:887–900, Dove Press.

Gnewuch C, Liebisch G, Langmann T, Dieplinger B, Mueller T, Haltmayer M, Dieplinger H, Zahn A, Stremmel W, Rogler G, and Schmitz G (2009) Serum bile acid profiling reflects enterohepatic detoxification state and intestinal barrier function in inflammatory bowel disease. *World J Gastroenterol* **15**:3134–41.

Guo C, Yang K, Brouwer KR, St Claire RL, and Brouwer KLR (2016) Prediction of Altered Bile Acid Disposition Due to Inhibition of Multiple Transporters: An Integrated Approach Using Sandwich-Cultured Hepatocytes, Mechanistic Modeling, and Simulation. *J Pharmacol Exp Ther* **358**:324–33.

Hartman JC, Brouwer K, Mandagere A, Melvin L, and Gorczynski R (2010) Evaluation of the endothelin receptor antagonists ambrisentan, darusentan, bosentan, and sitaxsentan as substrates and inhibitors of hepatobiliary transporters in sandwich-cultured human hepatocytes. *Can J Physiol Pharmacol* **88**:682–91.

Humbert M, Segal ES, Kiely DG, Carlsen J, Schwierin B, and Hoeper MM (2007) Results of

European post-marketing surveillance of bosentan in pulmonary hypertension. *Eur Respir J* **30**:338–44.

Humbert M, Sitbon O, and Simonneau G (2004) Treatment of pulmonary arterial hypertension. *N Engl J Med* **351**:1425–36.

Keemink J, Deferm N, De Bruyn T, Augustijns P, Bouillon T, and Annaert P (2018) Effect of Cryopreservation on Enzyme and Transporter Activities in Suspended and Sandwich Cultured Rat Hepatocytes. *AAPS J* **20**:33.

Kemp DC, Zamek-Gliszczynski MJ, and Brouwer KLR (2005) Xenobiotics inhibit hepatic uptake and biliary excretion of taurocholate in rat hepatocytes. *Toxicol Sci* **83**:207–14.

Lepist E-I, Gillies H, Smith W, Hao J, Hubert C, St Claire RL, Brouwer KR, and Ray AS (2014) Evaluation of the endothelin receptor antagonists ambrisentan, bosentan, macitentan, and sitaxsentan as hepatobiliary transporter inhibitors and substrates in sandwich-cultured human hepatocytes. *PLoS One* **9**:e87548.

Leslie EM, Watkins PB, Kim RB, and Brouwer KLR (2007) Differential inhibition of rat and human Na+-dependent taurocholate cotransporting polypeptide (NTCP/SLC10A1)by bosentan: a mechanism for species differences in hepatotoxicity. *J Pharmacol Exp Ther* **321**:1170–8.

Li R, Niosi M, Johnson N, Tess DA, Kimoto E, Lin J, Yang X, Riccardi KA, Ryu S, El-Kattan AF, Maurer TS, Tremaine LM, and Di L (2018) A Study on Pharmacokinetics of Bosentan with Systems Modeling, Part 1: Translating Systemic Plasma Concentration to Liver Exposure in Healthy Subjects. *Drug Metab Dispos* **46**:346–356, American Society for Pharmacology and Experimental Therapy.

Liu X, LeCluyse EL, Brouwer KR, Gan LS, Lemasters JJ, Stieger B, Meier PJ, and Brouwer KL

(1999) Biliary excretion in primary rat hepatocytes cultured in a collagen-sandwich configuration. *Am J Physiol* **277**:G12-21.

Mano Y, Usui T, and Kamimura H (2007) Effects of bosentan, an endothelin receptor antagonist, on bile salt export pump and multidrug resistance-associated protein 2. *Biopharm Drug Dispos* **28**:13–8.

Marion TL, Perry CH, St Claire RL, and Brouwer KLR (2012) Endogenous bile acid disposition in rat and human sandwich-cultured hepatocytes. *Toxicol Appl Pharmacol* **261**:1–9.

Markova SM, De Marco T, Bendjilali N, Kobashigawa EA, Mefford J, Sodhi J, Le H, Zhang C, Halladay J, Rettie AE, Khojasteh C, McGlothlin D, Wu AHB, Hsueh W-C, Witte JS, Schwartz JB, and Kroetz DL (2013) Association of CYP2C9*2 with bosentan-induced liver injury. *Clin Pharmacol Ther* **94**:678–86.

Matsson P, Pedersen JM, Norinder U, Bergström CAS, and Artursson P (2009) Identification of novel specific and general inhibitors of the three major human ATP-binding cassette transporters P-gp, BCRP and MRP2 among registered drugs. *Pharm Res* **26**:1816–31.

Matsui Y, Tu W, Kitade H, Nakagawa A, Kamiya T, Kwon AH, Uetsuji S, and Kamiyama Y (1996) Hepatocyte volume as an indicator of hepatic functional reserve in cirrhotic patients with liver tumours. *J Gastroenterol Hepatol* **11**:540–5.

Matuszewski BK, Constanzer ML, and Chavez-Eng CM (2003) Strategies for the assessment of matrix effect in quantitative bioanalytical methods based on HPLC-MS/MS. *Anal Chem* **75**:3019–30.

Morales-Navarrete H, Segovia-Miranda F, Klukowski P, Meyer K, Nonaka H, Marsico G, Chernykh M, Kalaidzidis A, Zerial M, and Kalaidzidis Y (2015) A versatile pipeline for the multi-scale digital reconstruction and quantitative analysis of 3D tissue architecture. *Elife* **4**.

Morgan RE, Trauner M, van Staden CJ, Lee PH, Ramachandran B, Eschenberg M, Afshari CA, Qualls CW, Lightfoot-Dunn R, and Hamadeh HK (2010) Interference with bile salt export pump function is a susceptibility factor for human liver injury in drug development. *Toxicol Sci* **118**:485–500, Oxford University Press.

Morgan RE, van Staden CJ, Chen Y, Kalyanaraman N, Kalanzi J, Dunn RT, Afshari CA, and Hamadeh HK (2013) A multifactorial approach to hepatobiliary transporter assessment enables improved therapeutic compound development. *Toxicol Sci* **136**:216–41, Oxford University Press.

Nakau K, Sugimoto M, Oka H, Kajihama A, Maeda J, Yamagishi H, Kamiyama N, Tasaki Y, Kajino H, and Azuma H (2016) Pharmacokinetics of drugs for pediatric pulmonary hypertension. *Pediatr Int* **58**:1112–1117.

Ogimura E, Nakagawa T, Deguchi J, Sekine S, Ito K, and Bando K (2017) Troglitazone Inhibits Bile Acid Amidation: A Possible Risk Factor for Liver Injury. *Toxicol Sci* **158**:347–355.

Oorts M, Baze A, Bachellier P, Heyd B, Zacharias T, Annaert P, and Richert L (2016) Drug-induced cholestasis risk assessment in sandwich-cultured human hepatocytes. *Toxicol In Vitro* **34**:179–86, Elsevier B.V.

Oshio C, and Phillips MJ (1981) Contractility of bile canaliculi: implications for liver function. *Science* **212**:1041–2.

Parmentier C, Hendriks DFG, Heyd B, Bachellier P, Ingelman-Sundberg M, and Richert L (2018) Inter-individual differences in the susceptibility of primary human hepatocytes towards drug-induced cholestasis are compound and time dependent. *Toxicol Lett* **295**:187–194.

Pfeifer ND, Yang K, and Brouwer KLR (2013) Hepatic basolateral efflux contributes

significantly to rosuvastatin disposition I: characterization of basolateral versus biliary clearance using a novel protocol in sandwich-cultured hepatocytes. *J Pharmacol Exp Ther* **347**:727–36.

Phillips MJ, Oshio C, Miyairi M, Katz H, and Smith CR (1982) A study of bile canalicular contractions in isolated hepatocytes. *Hepatology* **2**:763–8.

Rodrigues RM, Kollipara L, Chaudhari U, Sachinidis A, Zahedi RP, Sickmann A, Kopp-Schneider A, Jiang X, Keun H, Hengstler J, Oorts M, Annaert P, Hoeben E, Gijbels E, De Kock J, Vanhaecke T, Rogiers V, and Vinken M (2018) Omics-based responses induced by bosentan in human hepatoma HepaRG cell cultures. *Arch Toxicol* **92**:1939–1952.

Scherer M, Gnewuch C, Schmitz G, and Liebisch G (2009) Rapid quantification of bile acids and their conjugates in serum by liquid chromatography-tandem mass spectrometry. *J Chromatogr B Analyt Technol Biomed Life Sci* **877**:3920–5.

Sokol RJ, Dahl R, Devereaux MW, Yerushalmi B, Kobak GE, and Gumpricht E (2005) Human hepatic mitochondria generate reactive oxygen species and undergo the permeability transition in response to hydrophobic bile acids. *J Pediatr Gastroenterol Nutr* **41**:235–43.

Soroka CJ, Lee JM, Azzaroli F, and Boyer JL (2001) Cellular localization and up-regulation of multidrug resistance-associated protein 3 in hepatocytes and cholangiocytes during obstructive cholestasis in rat liver. *Hepatology* **33**:783–91.

Su T, and Waxman DJ (2004) Impact of dimethyl sulfoxide on expression of nuclear receptors and drug-inducible cytochromes P450 in primary rat hepatocytes. *Arch Biochem Biophys* **424**:226–34.

Swift B, Pfeifer ND, and Brouwer KLR (2010) Sandwich-cultured hepatocytes: an in vitro model to evaluate hepatobiliary transporter-based drug interactions and hepatotoxicity.

Drug Metab Rev **42**:446–71.

Thakare R, Alamoudi JA, Gautam N, Rodrigues AD, and Alnouti Y (2018) Species differences in bile acids II. Bile acid metabolism. *J Appl Toxicol* **38**:1336–1352.

Treiber A, Schneiter R, Häusler S, and Stieger B (2007) Bosentan is a substrate of human OATP1B1 and OATP1B3: Inhibition of hepatic uptake as the common mechanism of its interactions with cyclosporin A, rifampicin, and sildenafil. *Drug Metab Dispos* **35**:1400–1407.

Van Brantegem P, Chatterjee S, De Bruyn T, Annaert P, and Deferm N (2020) Drug-induced cholestasis assay in primary hepatocytes. *MethodsX* **7**:101080.

Woolbright BL, and Jaeschke H (2015) Critical Factors in the Assessment of Cholestatic Liver Injury In Vitro. *Methods Mol Biol* **1250**:363–76.

Xiang X, Han Y, Neuvonen M, Laitila J, Neuvonen PJ, and Niemi M (2010) High performance liquid chromatography-tandem mass spectrometry for the determination of bile acid concentrations in human plasma. *J Chromatogr B Analyt Technol Biomed Life Sci* **878**:51–60.

Xu D, Wu M, Nishimura S, Nishimura T, Michie SA, Zheng M, Yang Z, Yates AJ, Day JS, Hillgren KM, Takeda ST, Guan Y, Guo Y, and Peltz G (2015) Chimeric TK-NOG mice: a predictive model for cholestatic human liver toxicity. *J Pharmacol Exp Ther* **352**:274–80.

Yang K, Pfeifer ND, Köck K, and Brouwer KLR (2015) Species differences in hepatobiliary disposition of taurocholic acid in human and rat sandwich-cultured hepatocytes: implications for drug-induced liver injury. *J Pharmacol Exp Ther* **353**:415–23.

Yerushalmi B, Dahl R, Devereaux MW, Gumpricht E, and Sokol RJ (2001) Bile acid-induced rat hepatocyte apoptosis is inhibited by antioxidants and blockers of the mitochondrial

permeability transition. *Hepatology* **33**:616–26.

JPET Fast Forward. Published on August 4, 2021 as DOI: 10.1124/jpet.121.000695
This article has not been copyedited and formatted. The final version may differ from this version.

Footnotes

This research was supported by a research grant of the Research Foundation Flanders (grant number G012318N). ED is a postdoctoral research fellow of the Research Foundation Flanders (FWO), Belgium (grant number 12X9420N).

JPET Fast Forward. Published on August 4, 2021 as DOI: 10.1124/jpet.121.000695
This article has not been copyedited and formatted. The final version may differ from this version.

Figure legends

Figure 1. Interaction of bosentan with hepatic transporters and metabolic enzymes involved in bile salt homeostasis. Green arrows indicate that bosentan is a substrate for that particular transport protein or enzyme, while red inhibition signs illustrate the inhibitory effect of bosentan. (A) (Treiber *et al.*, 2007); (B) (Lepist *et al.*, 2014); (C) (Leslie *et al.*, 2007); (D) (Morgan *et al.*, 2010; Dawson *et al.*, 2012); (E) (Mano *et al.*, 2007); (F) (Morgan *et al.*, 2013); (G) (Fouassier *et al.*, 2002); (H) (Matuszewski *et al.*, 2003).

Figure 2. Scheme illustrating the incubations performed in sandwich-cultured human hepatocytes (SCHH). (A) Incubation protocol to investigate the effect of bosentan on the endogenous bile salts. (B) Representation of the accumulation study in the presence of 10 µM CDCA. Four sampling times (indicated by arrows) were performed, namely culture medium present on the hepatocytes (1), culture medium at time 0 (2), culture medium after the loading phase (3) and cell lysates (4). (C) Representation of the efflux study in the presence of 10 µM CDCA. In this setup, 5 sampling times were performed: culture medium present on the hepatocytes (1), culture medium at time 0 (2), culture medium after the loading phase (3), buffer samples after efflux phase (4) and cell lysates (5).

Figure 3. Mechanistic model used to describe the data. (A) Predetermined structural model used to estimate the parameters involved in CDCA and GCDCA disposition. (B) Observed and simulated amounts of CDCA and GCDCA in each compartment for different bosentan concentrations. The solid black line indicates the mean amounts. The grey lines indicate the 95%

JPET Fast Forward. Published on August 4, 2021 as DOI: 10.1124/jpet.121.000695
This article has not been copyedited and formatted. The final version may differ from this version.

prediction interval. For compartments 3 and 4, all possible calculated amounts for the imputation procedure are depicted.

Figure 4. The relative amount (% of control) of the endogenous bile salts GCDCA and GCA present in the culture medium (A, B, C, D) or in the lysate of cells and canaliculi combined (E, F) of SCHH. Samples were taken at day 6 of culture time in absence (0.2% DMSO, black) or presence of bosentan (25 μM, white). (A, B) Exposure periods were 0.5 h, 4 h and 24 h. Other bile salts were not detected in the medium as analyzed by LC-MS/MS (LLOQ = 9.8 nM). (C, D) Exposure periods were 0.5 h followed by a recovery phase of 23.5 h and 4 h followed by a recovery phase of 20 h (total incubation time of 24 h). (E, F) Exposure periods were 0.5 h followed by a recovery phase of 23.5 h, 4 h followed by a recovery phase of 20 h, and 24 h. Bars represent mean (± SD) of the amount (pmol) of GCDCA and GCA in two batches of human hepatocytes (3 and 4 replicates from donor n°1 and 2, respectively). Conditions were compared to the control condition using a two-tailed unpaired t-test (*$p < 0.05$, **$p < 0.01$ and ***$p < 0.001$).

Figure 5. Time-dependent accumulation of (A) CDCA (10 μM) and (B) GCDCA in cells and canaliculi of SCHH after various exposure periods (0.5, 1, 4, 12 and 24 h) with 10 μM CDCA in absence (closed circles) or in presence of bosentan (7.5 μM: open circles and 25 μM: triangles). Each point represents mean (± SD) accumulation of bile salts obtained from triplicate measurements in one batch of SCHH (donor n°3). Conditions were compared to the control condition (i.e., closed circles) (*$p < 0.05$, **$p < 0.01$ and ***$p < 0.001$).

JPET Fast Forward. Published on August 4, 2021 as DOI: 10.1124/jpet.121.000695
This article has not been copyedited and formatted. The final version may differ from this version.

Figure 6. Efflux and efflux clearances of GCDCA observed in SCHH in absence and presence of bosentan. (A, B, C, D) Efflux of GCDCA from SCHH as measured over a 15 min efflux experiment following various loading periods (0.5, 1, 4, 12 and 24 h) with 10 µM CDCA in absence (control: A) or presence of bosentan (2.5 µM: B, 7.5 µM: C and 25 µM: D). After each loading time, a 15 min efflux phase was initiated with either standard (sinusoidal efflux: closed circles) or Ca^{2+}/Mg^{2+}-free buffer (total efflux: open circles) and buffer samples were analyzed. Data obtained in standard buffer were subtracted from data obtained in Ca^{2+}/Mg^{2+}-free buffer to account for canalicular efflux (triangles). Each point represents mean (± SD) accumulation in buffers of bile salts obtained from four measurements in one batch of SCHH (donor n°3). (E) Sinusoidal and (F) canalicular efflux clearance (nL/min) of GCDCA observed in SCHH in absence or presence of bosentan (7.5 and 25 µM) and an efflux phase for 15 min. Sinusoidal and canalicular efflux clearances are calculated as described in the Materials and Methods. Bars represent mean (± SD) efflux clearance values of GCDCA in one batch of SCHH (donor n°3) with quadruplicate measurements. Conditions were compared to the control condition (*$p < 0.05$, **$p < 0.01$ and ***$p < 0.001$).

Figure 7. Effect of several bosentan concentrations on the glycine conjugation of CDCA to GCDCA in liver S9 fraction. Bosentan reduced GCDCA formation in the presence of 85 µM and 250 µM bosentan when incubated for 60 min with both 10 µM and 50 µM CDCA.

JPET Fast Forward. Published on August 4, 2021 as DOI: 10.1124/jpet.121.000695
This article has not been copyedited and formatted. The final version may differ from this version.

Tables

Table 1. AUC values representing accumulation of CDCA and GCDCA in cells and canaliculi of SCHH in absence or presence of bosentan, based on measurements obtained after various loading periods (0.5, 1, 4, 12 and 24 h) with 10 µM CDCA. The data presented in Figure 5 were used to calculate the AUC values by means of the trapezoidal rule. Conditions were compared to the control condition (*$p < 0.05$, **$p < 0.01$ and ***$p < 0.001$).

Conditions	**AUC of CDCA ± SD (pmol*h)**	**AUC of GCDCA ± SD (pmol*h)**
Control	254 ± 30	4809 ± 250
7.5 µM bosentan	263 ± 44	3437 ± 391 (**)
25 µM bosentan	299 ± 6	2541 ± 159 (***)

AUC, area under the curve; CDCA, chenodeoxycholic acid; GCDCA, glycochenodeoxycholic acid.

JPET Fast Forward. Published on August 4, 2021 as DOI: 10.1124/jpet.121.000695
This article has not been copyedited and formatted. The final version may differ from this version.

Table 2. AUC values representing sinusoidal, canalicular and total efflux of GCDCA by SCHH, measured over 15 min following various loading periods (0.5, 1, 4, 12 and 24 h) with 10 µM CDCA in absence or presence of bosentan. The data in Figure 6A-D were used to calculate the AUC values by means of the trapezoidal rule. Conditions were compared to the control condition (*$p < 0.05$, **$p < 0.01$ and ***$p < 0.001$).

	AUC of GCDCA ± SD (pmol*h)		
Conditions	**Total efflux**	**Sinusoidal efflux**	**Canalicular efflux**
Control	2654 ± 535	1170 ± 251	1474 ± 409
2.5 µM bosentan	2367 ± 145	1277 ± 19	1080 ± 156
7.5 µM bosentan	1750 ± 247 (**)	973 ± 45	718 ± 243 (**)
25 µM bosentan	1411 ± 104 (***)	956 ± 88	418 ± 43 (***)

AUC, area under the curve; GCDCA, glycochenodeoxycholic acid.

JPET Fast Forward. Published on August 4, 2021 as DOI: 10.1124/jpet.121.000695
This article has not been copyedited and formatted. The final version may differ from this version.

Table 3. Effect of bosentan as a categorical covariate on different model parameters.

Model	OFV	dOFV
Base	5738.9	-
Base + $CL_{bile,GCDCA}$	5728.2	-10.7
Base + $CL_{eff,GCDCA}$	5729.3	-9.6
Base + $CL_{met,CDCA}$	5738.3	-0.6
Base + $CL_{bile,GCDCA}$ and $CL_{eff,GCDCA}$	5722.2	-16.8

dOFV, drop in OFV; OFV, objective function value.

JPET Fast Forward. Published on August 4, 2021 as DOI: 10.1124/jpet.121.000695
This article has not been copyedited and formatted. The final version may differ from this version.

Table 4. Median population estimates and residual error with 95% confidence interval (CI) after 4,495 successful imputations.

Parameter	Population estimate	95% CI
$K_{m,up,CDCA}$ (µM)	4.77	4.61-4.93
$V_{max,up,CDCA}$ (pmol/min)	5.19	5.08-5.31
$CL_{met,CDCA}$ (µL/min)	0.186	0.179-0.192
$CL_{bile,GCDCA}$ (control condition) (µL/min)	0.014	0.012-0.017
$CL_{bile,GCDCA}$ (2.5 µM bosentan) (µL/min)	0.011	0.009-0.014
$CL_{bile,GCDCA}$ (7.5 µM bosentan) (µL/min)	0.013	0.007-0.017
$CL_{bile,GCDCA}$ (25 µM bosentan) (µL/min)	0.006	0.003-0.009
$CL_{eff,GCDCA}$ (µL/min)	0.049	0.047-0.051
$CL_{up,GCDCA}$ (µL/min)	0.230	0.207-0.256
k_{flux} (min^{-1})	0.012	0.010-0.014
Proportional error (%CV)		
Compartments 1 and 5	8.3	8.2-8.4
Compartments 2, 3 and 4	24.4	21.0-27.6
Additive error (pmol)		
Compartment 2	72.1	50.1-93.3
Compartment 4	3.49	3.04-4.14

Figure 1

JPET Fast Forward. Published on August 4, 2021 as DOI: 10.1124/jpet.121.000695
This article has not been copyedited and formatted. The final version may differ from this version.

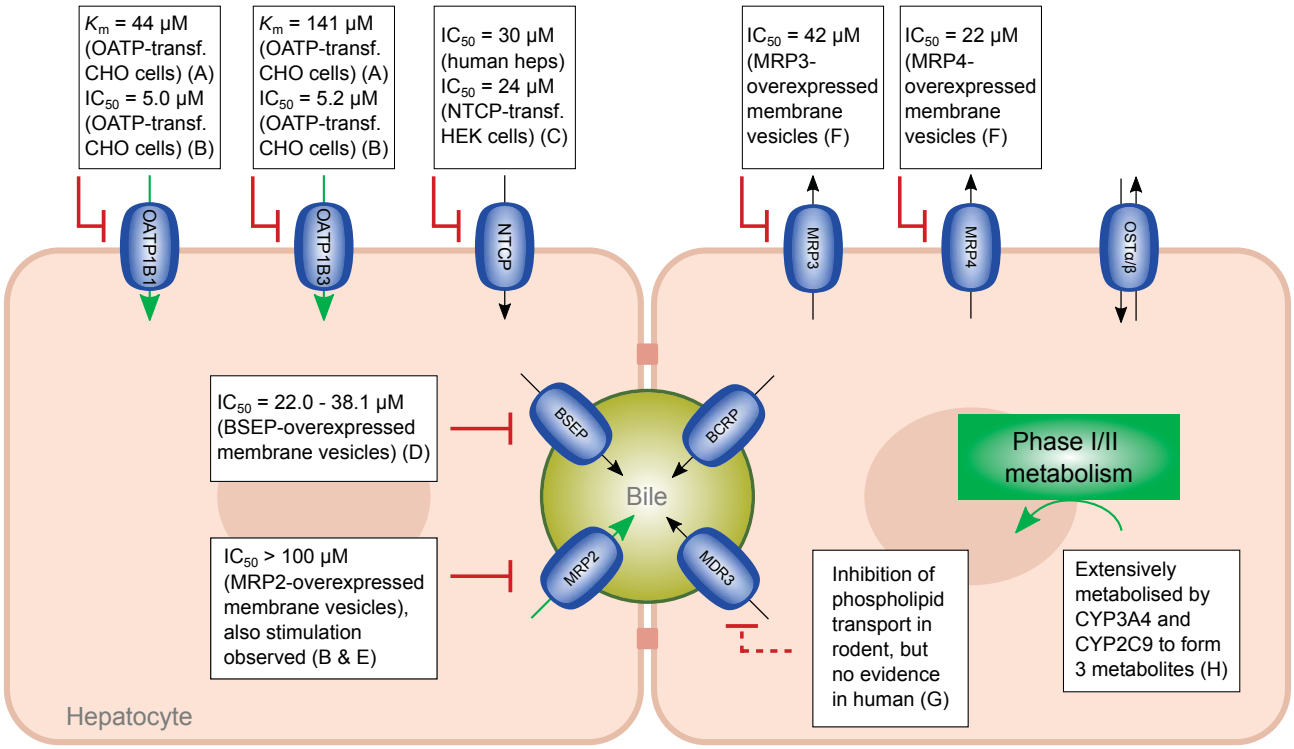

Figure 2

JPET Fast Forward. Published on August 4, 2021 as DOI: 10.1124/jpet.121.000695
This article has not been copyedited and formatted. The final version may differ from this version.

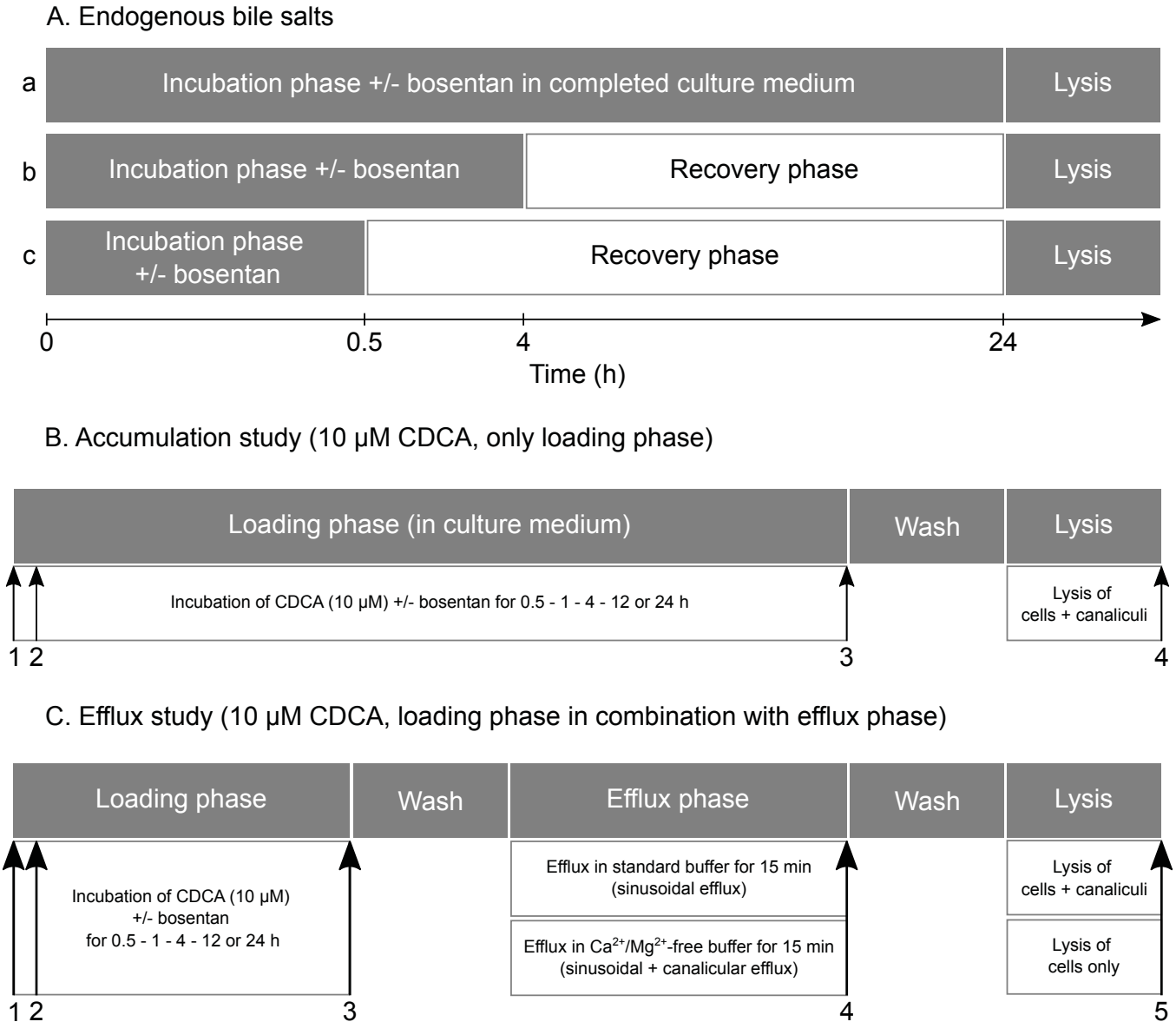

Figure 3

JPET Fast Forward. Published on August 4, 2021 as DOI: 10.1124/jpet.121.000695
This article has not been copyedited and formatted. The final version may differ from this version.

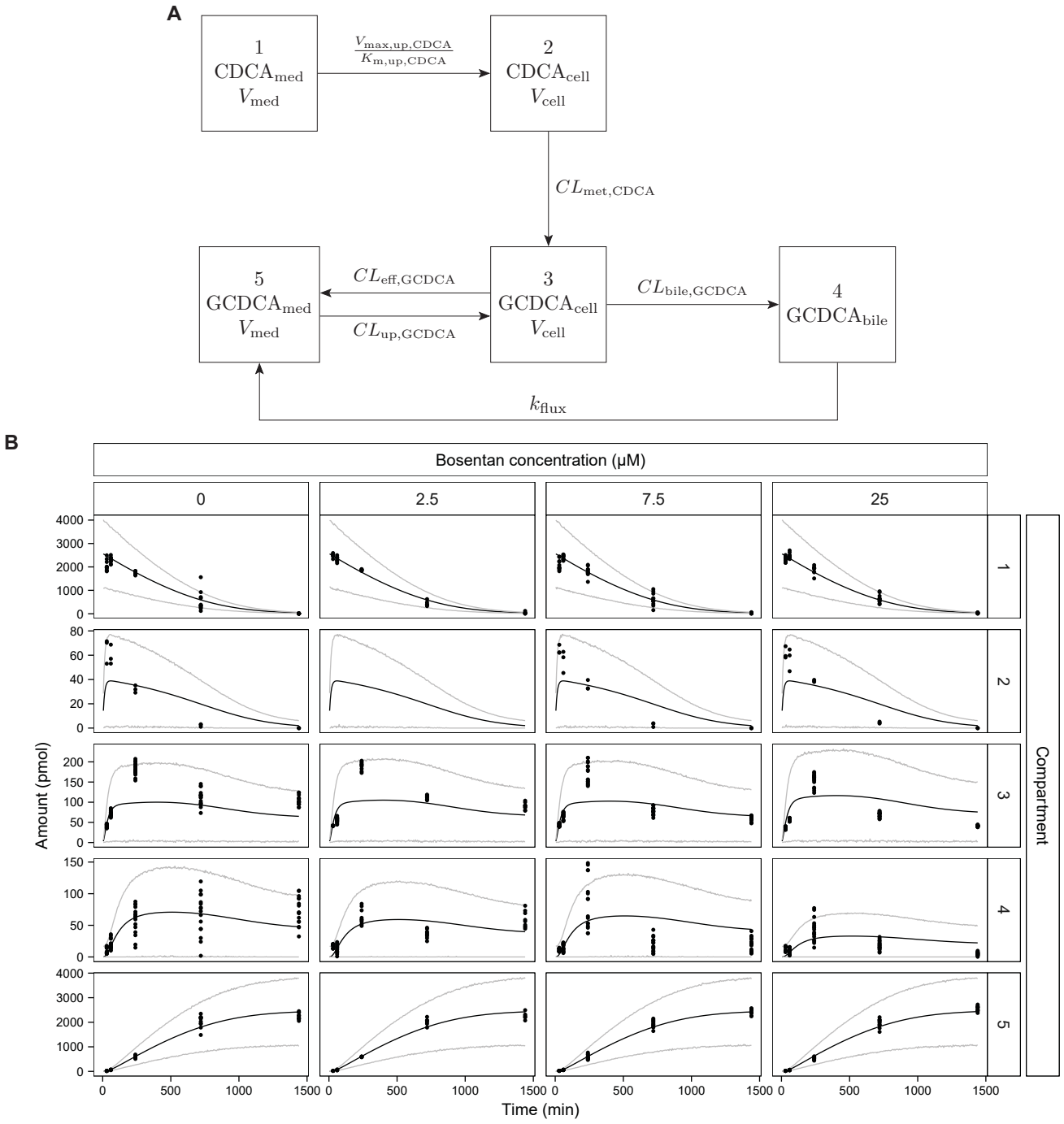

Figure 4

JPET Fast Forward. Published on August 4, 2021 as DOI: 10.1124/jpet.121.000695
This article has not been copyedited and formatted. The final version may differ from this version.

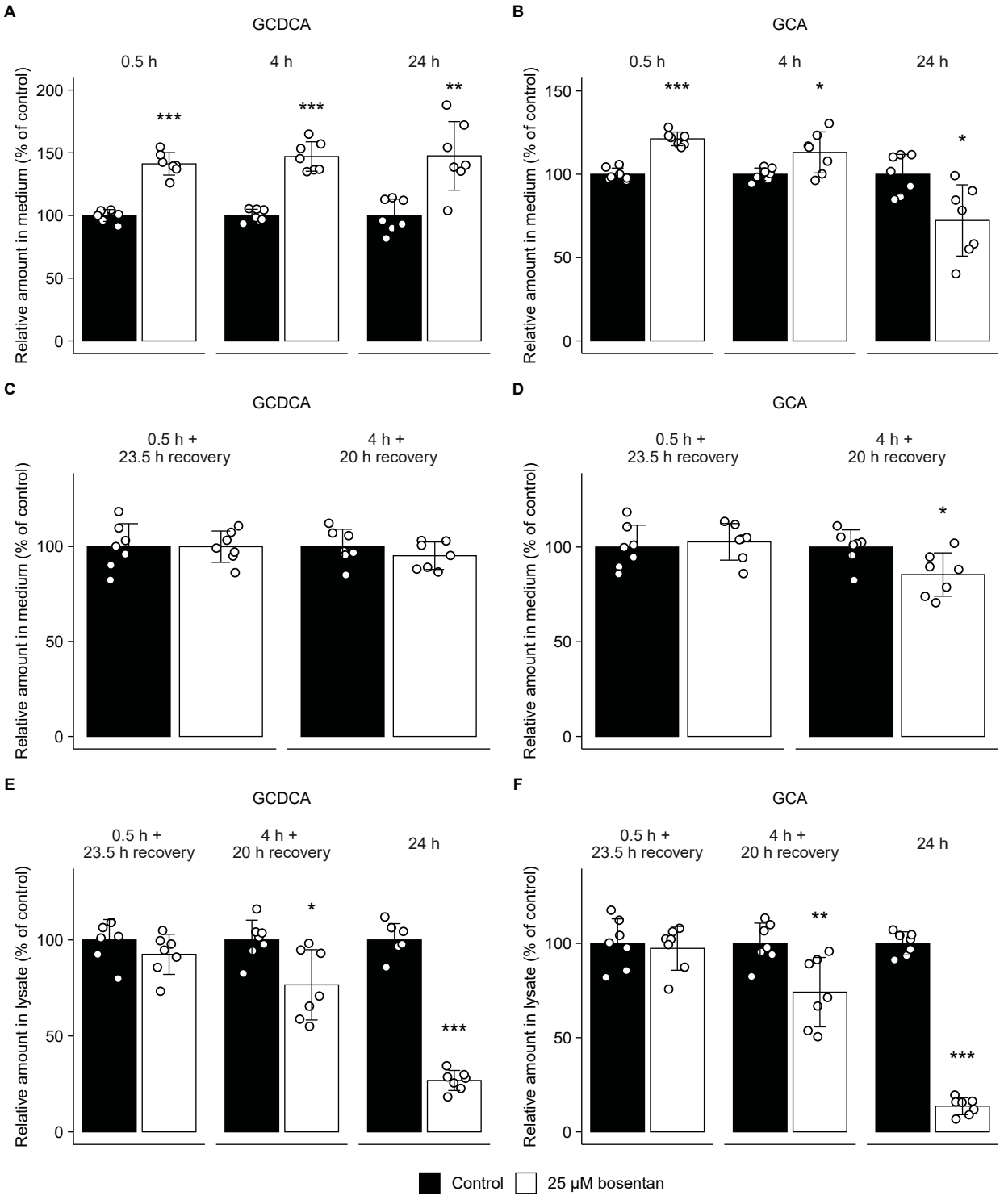

Figure 5

JPET Fast Forward. Published on August 4, 2021 as DOI: 10.1124/jpet.121.000695
This article has not been copyedited and formatted. The final version may differ from this version.

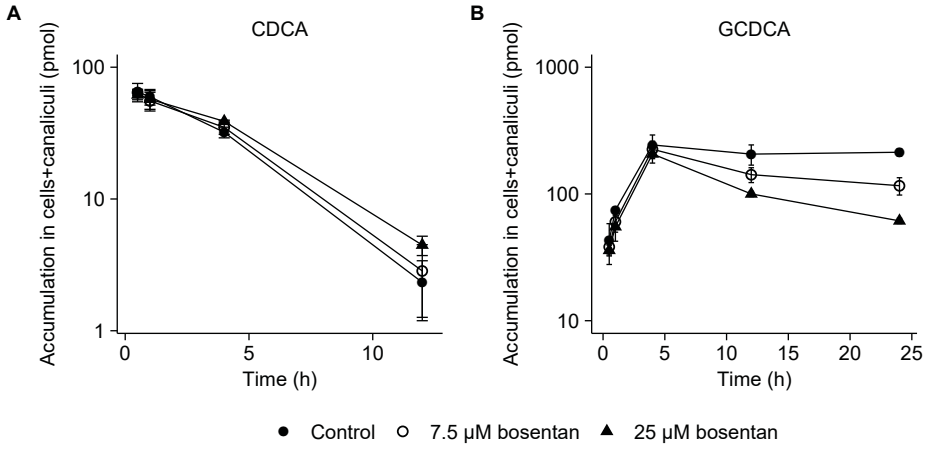

Figure 6

JPET Fast Forward. Published on August 4, 2021 as DOI: 10.1124/jpet.121.000695
This article has not been copyedited and formatted. The final version may differ from this version.

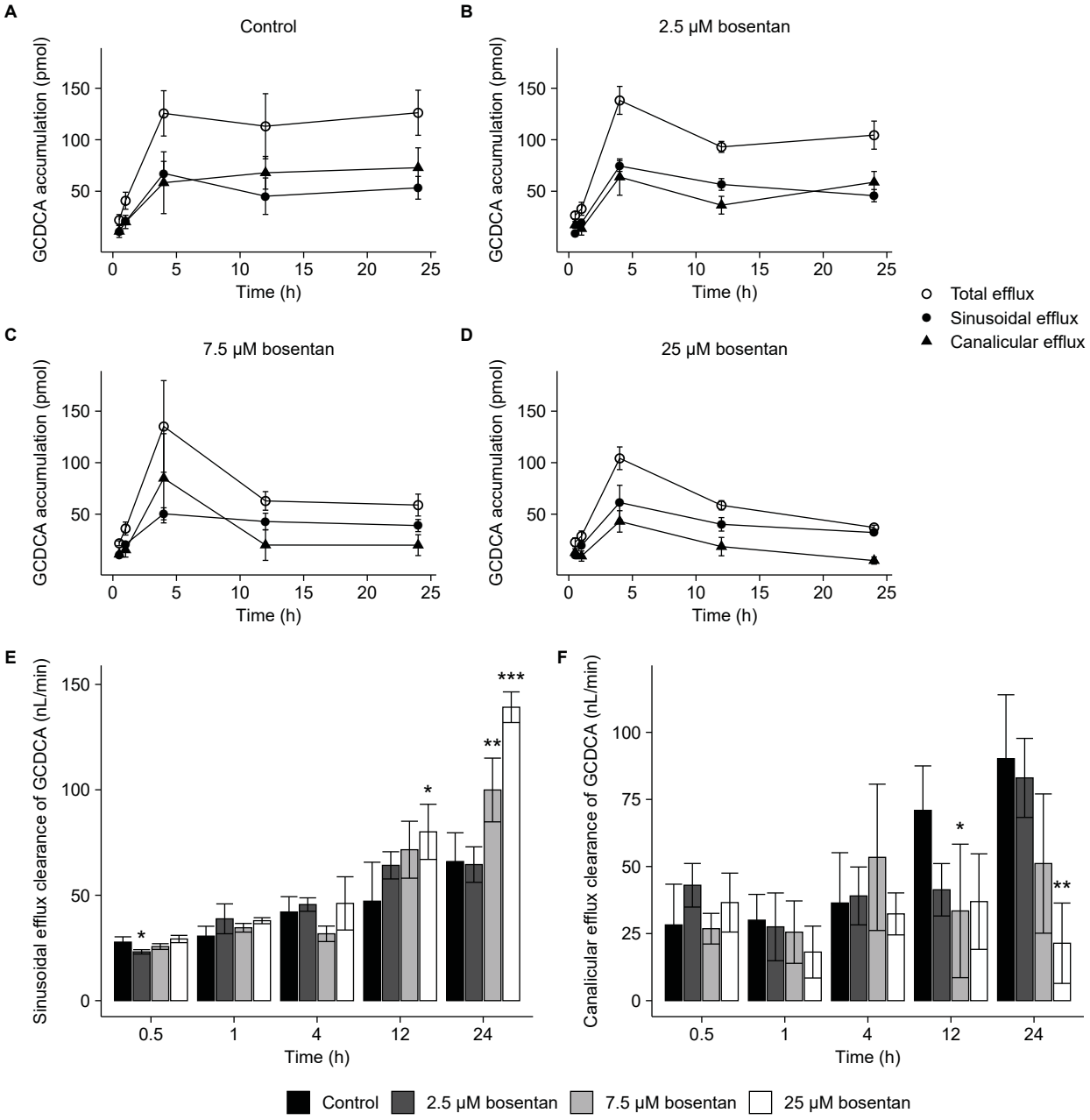

Figure 7

JPET Fast Forward. Published on August 4, 2021 as DOI: 10.1124/jpet.121.000695
This article has not been copyedited and formatted. The final version may differ from this version.

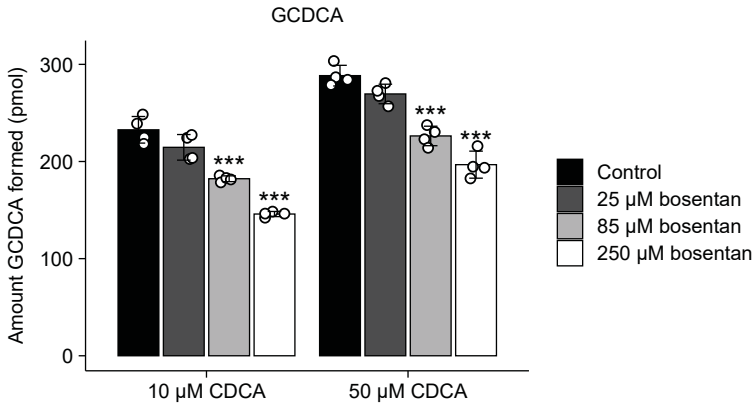

Supplemental Data

Bosentan alters endo- and exogenous bile salt disposition in sandwich-cultured human hepatocytes

The Journal of Pharmacology and Experimental Therapeutics

JPET-AR-2021-000695

Marlies Oorts*, Pieter Van Brantegem*, Neel Deferm, Sagnik Chatterjee, Erwin Dreesen, Axelle Cooreman, Mathieu Vinken, Lysiane Richert, Pieter Annaert

* Shared first authorship

Drug Delivery and Disposition, Department of Pharmaceutical and Pharmacological Sciences, KU Leuven, Leuven, Belgium: MO, PVB, ND, PA
Pharmaceutical Candidate Optimization, Biocon Bristol-Myers Squibb Research Center, Syngene International, Bangalore, India: SC
Clinical Pharmacology and Pharmacotherapy, Department of Pharmaceutical and Pharmacological Sciences, KU Leuven, Leuven, Belgium: ED
Uppsala Pharmacometrics Research Group, Department of Pharmacy, Uppsala University, Uppsala, Sweden: ED
Department of Pharmaceutical and Pharmacological Sciences, Vrije Universiteit Brussel, Brussels, Belgium: AC, MV
KaLy-Cell, Plobsheim, France: LR
BioNotus, Niel, Belgium: PA

Supplementary Methods

Materials

Bosentan hydrate was obtained from Carbosynth Limited (Berkshire, UK). Dimethyl sulfoxide (DMSO) and methanol (MeOH) were purchased from Acros Organics (Geel, Belgium). All bile salts, recombinant human insulin, 5-(6)-carboxy-2',7'-dichlorofluorescein diacetate (CDFDA), Percoll®, ethylene glycol-bis(β-aminoethyl ether)-N,N,N',N'-tetraacetic acid (EGTA), ammonium acetate and dexamethasone were all acquired from Sigma-Aldrich (Schnelldorf, Germany). Williams' E Medium (WEM), Dulbecco's modified eagle's medium (DMEM), L-glutamine (200 mM), penicillin–streptomycin mixture (containing 10,000 IU potassium penicillin and 10,000 μg streptomycin sulfate per mL in 0.85% saline), Trypan blue stain (0.4%), 1× and 10× phosphate-buffered saline (PBS), Hanks' balanced salt solution (HBSS) (referred to as standard buffer with pH adjusted to 7.4), Ca^{2+}/Mg^{2+}-free HBSS, ECM gel and fetal bovine serum (FBS) were obtained from Lonza Westburg BV (Leusden, The Netherlands). ITS+™ Premix was purchased from BD Biosciences (Erembodegem, Belgium). Acetonitrile (ACN) and acetic acid were acquired from Analar-Normapur (VWR) (Leicestershire, England). HEPES was purchased from MP Biochemical (Illkirch, France). Cholic acid-2,2,4,4-d4 (CA-d4) was obtained from Ritmeester BV (Nieuwegein, The Netherlands). Pooled human liver S9 fraction from 100 male and 100 female donors were purchased from XenoTech (Kansas City, KS, USA).

Sandwich-cultured human hepatocytes

Hepatocytes were cultured in a sandwich configuration as described previously with slight modifications (Oorts et al., 2016). To start, plastic 48-well sterile cell culture plates with a surface of 0.95 cm^2 (Greiner Bio One, Wemmel, Belgium) were coated one day before seeding with 50 μg/mL rigid collagen diluted in 0.02 N acetic acid (250 μL/well) and placed overnight at 37°C in a humidified atmosphere with 5% CO2. After thawing, the cells were resuspended in seeding medium (consisting of WEM supplemented with 10% FBS, 100 IU/mL penicillin, 100 μg/mL streptomycin, 2 mM L-glutamine, 4 μg/mL insulin and 1 μM dexamethasone). Hepatocytes were counted using a hemocytometer and cell viability was determined using Trypan blue. Cells were further diluted to a final concentration of 1×10^6 cells/mL and cells were subsequently seeded with a density of 0.25×10^6 viable cells/well. The hepatocyte monolayers were overlaid 24 h after seeding with Matrigel® (0.25 mg/mL) in ice-cold culture medium (WEM medium containing 1% (v/v) ITS+™ Premix, 2 mM L-glutamine, 100 IU/mL penicillin, 100 μg/mL streptomycin, and 0.1 μM dexamethasone). Medium was changed daily with pre-warmed culture medium. At day 3 of culture time, cells were overlaid for a second time with Matrigel® (0.25 mg/mL) diluted in ice-cold culture medium. Light microscopic images of the SCHH were taken on a daily basis.

Determination of fu

Unbound fractions of CDCA and GCDCA in hepatocytes ($fu_{\text{cell,CDCA}}$ and $fu_{\text{cell,GCDCA}}$) were determined by equilibrium dialysis using a HTDialysis apparatus (CT, USA) equipped with membranes with a molecular mass cutoff of 12-14 kDa. Cryopreserved human hepatocytes were thawed and diluted in culture medium to a final density of 0.5×10^6 cells/mL. Cells were then metabolically inactivated by heat (50°C, 15 min), after which their viability was determined using Trypan blue. The equilibrium dialysis experiments were performed under low circular shaking speed at 37°C. Samples were taken from the donor and acceptor compartments after at 4 h and 6 h. Experiments were performed in triplicate at CDCA and GCDCA concentrations of 10 μM (0.2% v/v DMSO).

Supplementary Figures

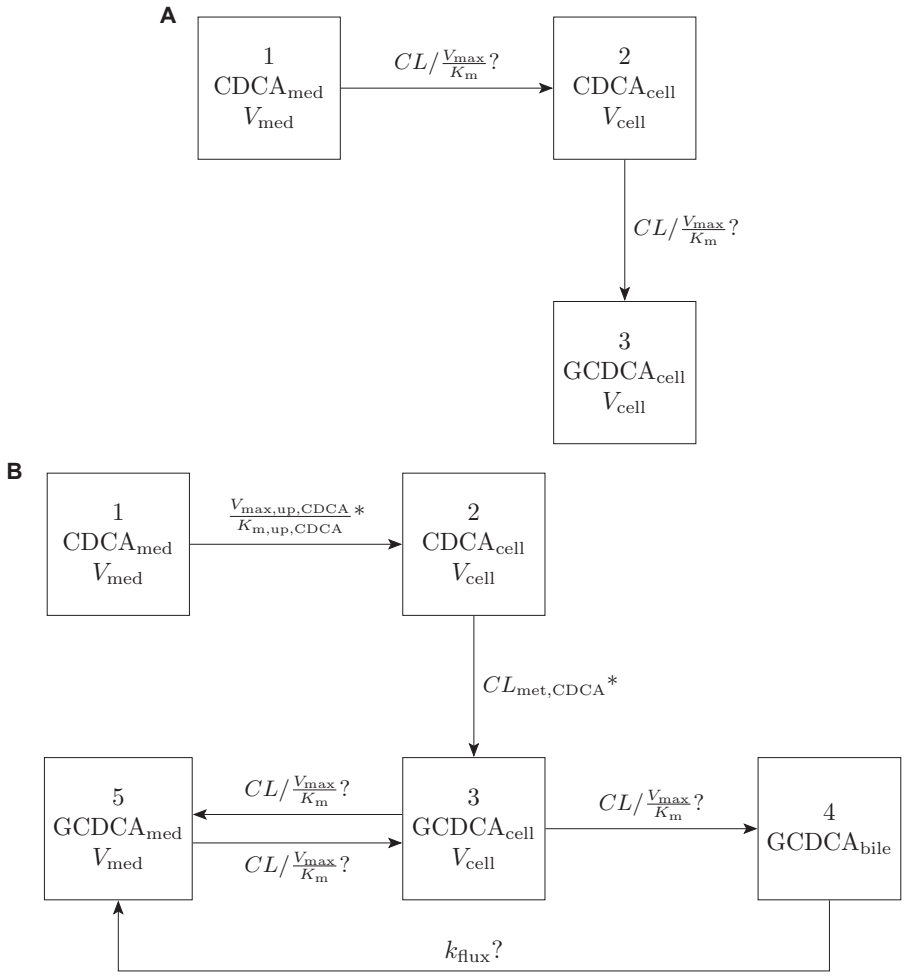

Supplementary Figure 1. Structural models used throughout the mechanistic modeling. (A) Model used for the first step of the mechanistic modeling. In this model, only uptake and metabolic clearance of CDCA was explored. GCDCA measured in all compartments was added up together in compartment 3. Both linear clearance and Michaelis-Menten kinetics were explored for uptake as well as metabolism of CDCA. (B) Model used for the second step of the mechanistic modeling. In this model, GCDCA disposition was explored while CDCA uptake and metabolic clearance parameters were fixed (indicated with an asterisk). Both linear clearance and Michaelis-Menten kinetics were explored. K_{flux} represents the periodic contractions of the bile canaliculi.

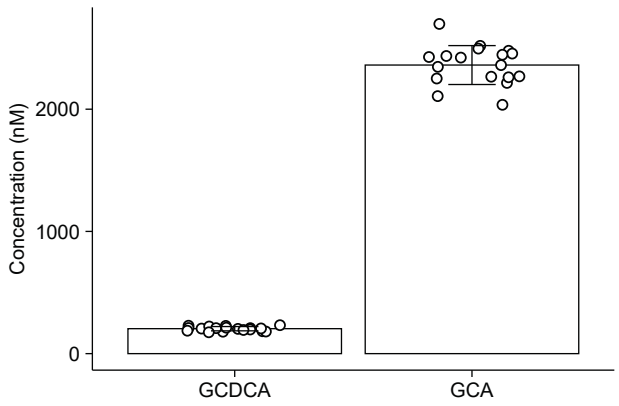

Supplementary Figure 2. The concentration of endogenous bile salts (GCDCA and GCA) present in the culture medium of SCHH at day 5 of culture time, not treated with bosentan. Other bile salts were not detected in the medium as analyzed by LC-MS/MS (LLOQ = 9.8 nM). Bars represent mean (± SD) of the concentration of GCDCA and GCA from 18 replicates in one batch of human hepatocytes (donor n°1).

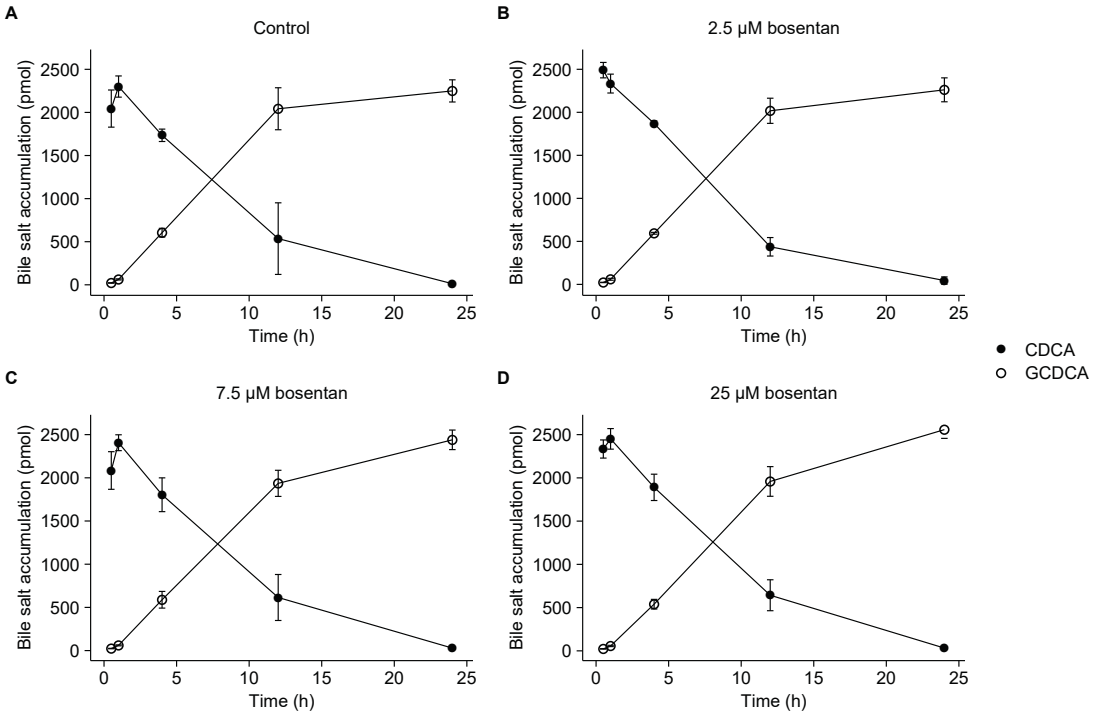

Supplementary Figure 3. Time-dependent levels of CDCA (10 μM; closed circles) and GCDCA (open circles) in the culture medium of SCHH for incubations in the absence (A) or presence of bosentan (2.5 μM: B; 7.5 μM: C and 25 μM: D). Each point represents mean (± SD) accumulation of bile salts obtained from 11 measurements in one batch of SCHH (donor n°3).

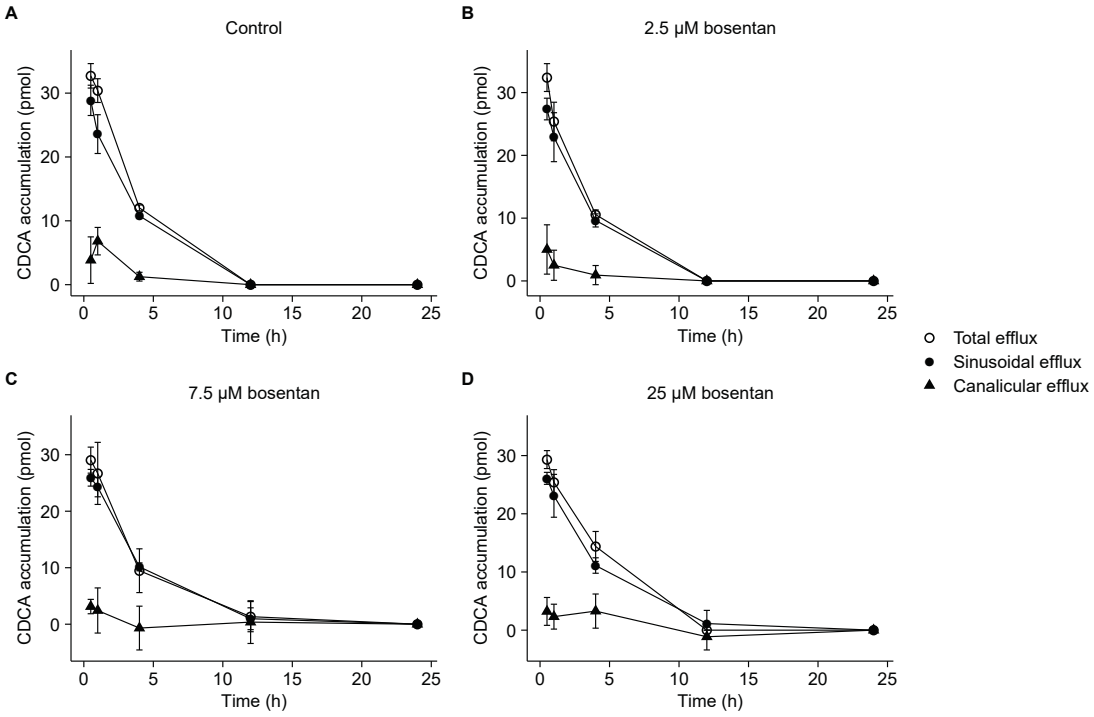

Supplementary Figure 4. Efflux of CDCA from SCHH as measured over a 15 min efflux experiment following various loading periods (0.5, 1, 4, 12 and 24 h) with CDCA in absence (A) or presence of bosentan (2.5 μM: B, 7.5 μM: C and 25 μM: D). After each loading period, a 15 min efflux phase was initiated with either standard (sinusoidal efflux: closed circles) or Ca^{2+}/Mg^{2+}-free buffer (total efflux: open circles) and buffer samples were analyzed. Data obtained in standard buffer was subtracted from data obtained in Ca^{2+}/Mg^{2+}-free buffer to account for canalicular efflux (triangles). Each point represents mean ($\pm$ SD) accumulation in buffers of bile salts obtained from four measurements in one batch of SCHH (donor n°3).

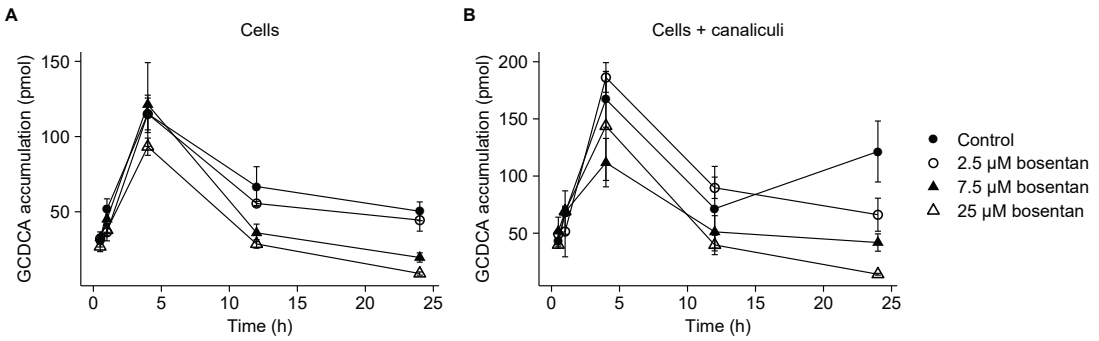

Supplementary Figure 5. Accumulated levels of GCDCA in SCHH as measured after various loading periods (0.5, 1, 4, 12 and 24 h) with CDCA and a subsequent efflux phase of 15 min, in absence (control: closed circles) or presence of bosentan (2.5 μM: open circles, 7.5 μM: closed triangles and 25 μM: open triangles). Lysates from cells after treatment with Ca^{2+}/Mg^{2+}-free buffer depict the intracellular amount of bile salts in cells (A), while lysates from cells after treatment with standard buffer depict the intracellular amount of bile salts in cells+canaliculi (B). Each point represents mean ($\pm$ SD) intracellular accumulation of bile salts obtained from four measurements in one batch of SCHH (donor n°3). Conditions were compared to the control condition (i.e., closed circles) (**$p < 0.01$ and ***$p < 0.001$).

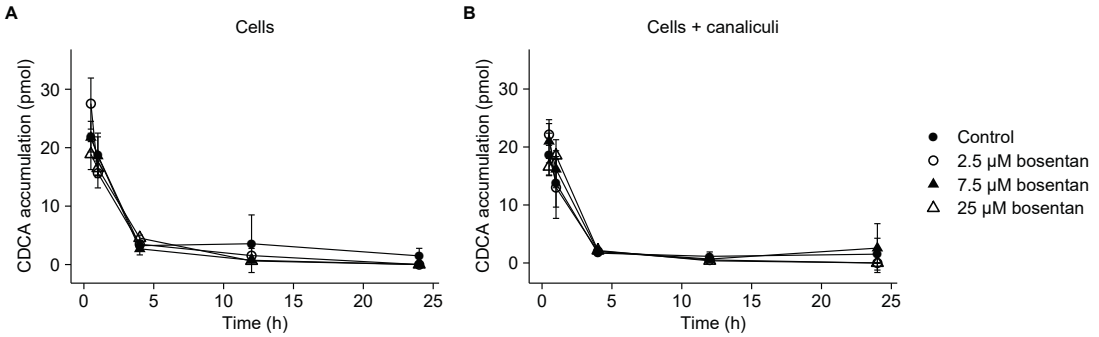

Supplementary Figure 6. Accumulated levels of CDCA in SCHH as measured after various loading periods (0.5, 1, 4, 12 and 24 h) with CDCA and a subsequent efflux phase of 15 min, in absence (control: closed circles) or presence of bosentan (2.5 μM: open circles, 7.5 μM: closed triangles and 25 μM: open triangles). Lysates from cells after treatment with Ca^{2+}/Mg^{2+}-free buffer depict the intracellular amount of bile salts in cells (A), while lysates from cells after treatment with standard buffer depict the intracellular amount of bile salts in cells+canaliculi (B). Each point represents mean ($\pm$ SD) intracellular accumulation of bile salts obtained from four measurements in one batch of SCHH (donor n°3).

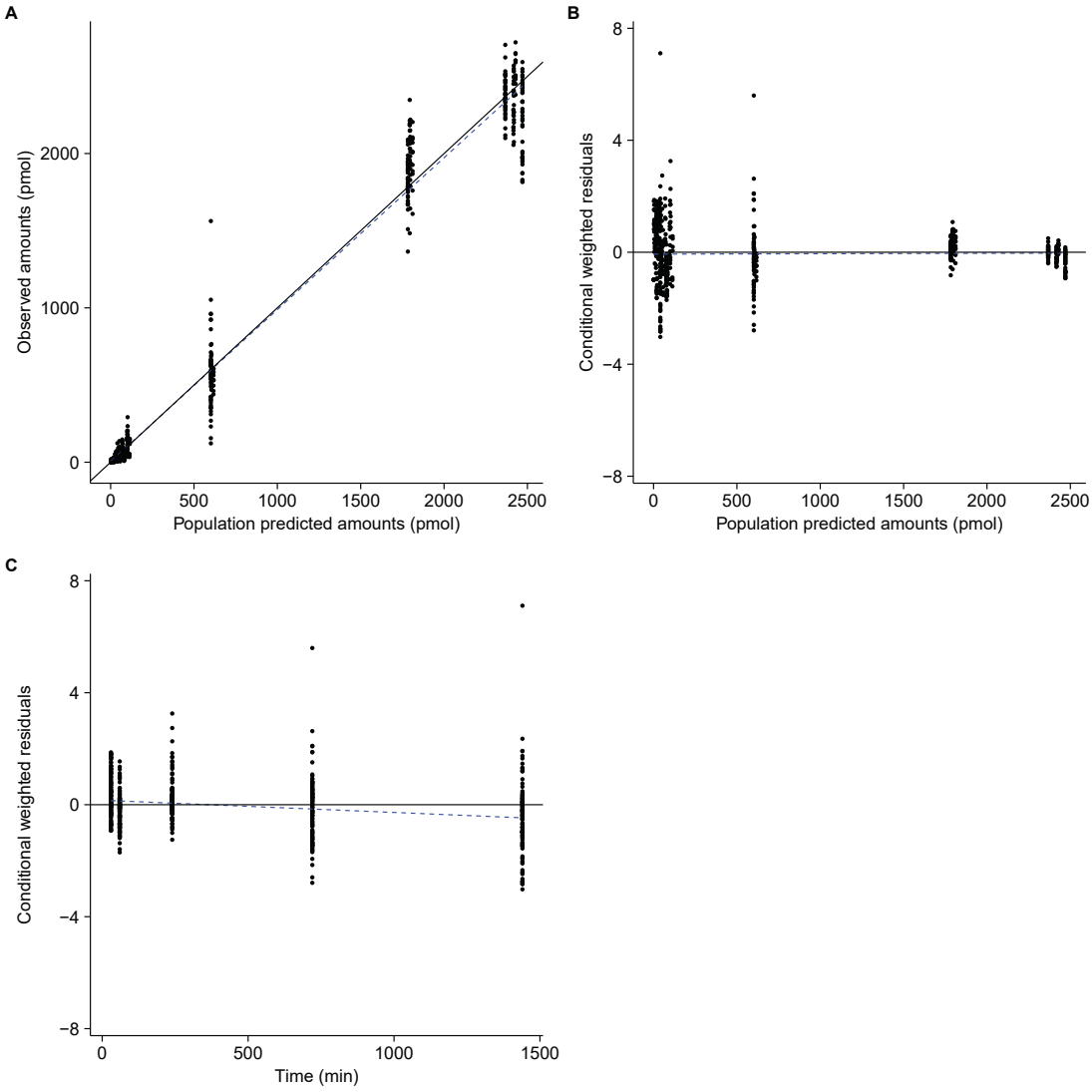

Supplementary Figure 7. The diagnostic plots of the final mechanistic model. (A) Observed CDCA and GCDCA amounts versus the population predicted CDCA and GCDCA amounts. (B) Conditional weighted residuals versus the population predicted amounts. (C) Conditional weighted residuals versus time. The blue dashed line indicates the trend line. The black line in (A) represents the line of identity.

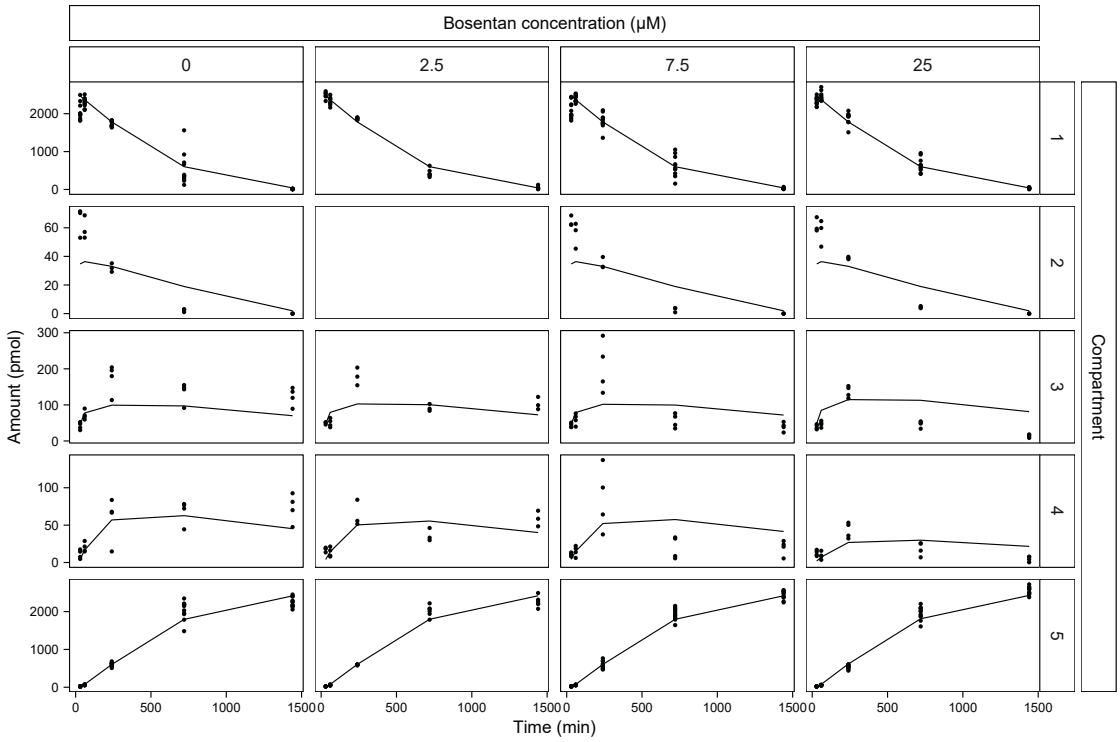

Supplementary Figure 8. Observed (closed circles) and population predicted (solid lines) amounts of CDCA and GCDCA in function of time per bosentan concentration and compartment. The compartment numbers correspond to the compartments as defined in Figure 3A.

Supplementary Tables

Supplementary Table 1. Demographics and donor characteristics of the cryopreserved human hepatocytes used throughout the study.

N°	Supplier	Donor name	Sex	Age	Pathology	Viability	Experiment
1	Kaly-Cell	M1394T	Female	58	Not known	89%	Endogenous bile salts
2	Kaly-Cell	S1356T	Female	59	Not known	89%	Endogenous bile salts
3	Kaly-Cell	S1386T	Female	60	Colorectal adenocarcinoma	87%	CDCA disposition

CDCA, chenodeoxycholic acid.

Supplementary Table 2. Mobile phase gradient of bile salt analysis on LC-MS/MS. The buffer consisted of 5 mM ammonium acetate (pH adjusted to 3.5 with acetic acid).

Time (min)	ACN (%)	MeOH (%)	H_2O (%)	Buffer (%)
0	0.0	5.0	91.0	4.0
0.5	0.0	5.0	91.0	4.0
1.0	13.0	48.0	35.0	4.0
5.0	13.0	48.0	35.0	4.0
7.0	19.0	48.0	29.0	4.0
8.9	19.0	48.0	29.0	4.0
9.0	33.0	48.0	15.0	4.0
10.4	33.0	48.0	15.0	4.0
10.5	0.0	5.0	91.0	4.0
12.0	0.0	5.0	91.0	4.0

ACN, acetonitrile; MeOH, methanol.

Supplementary Table 3. Parent and daughter m/z ratios and collision energies of the bile salts and internal standard CA-d4.

Bile salts	Parent m/z	Daughter m/z	Collision energy
TUDCA – TCDCA - TDCA	498.258	124.050	52
GUDCA – GCDCA – GDCA	448.275	74.250	43
TCA	514.257	124.050	52
GCA	464.269	74.250	41
UDCA – CDCA - DCA	391.256	-	0
CA	407.252	343.252	37
LCA	375.228	-	0
CA-d4	411.286	347.153	37

CA, cholic acid; CDCA, chenodeoxycholic acid; CA-d4, Cholic acid-2,2,4,4-d4; DCA, deoxycholic acid; GCA, glycocholic acid; GCDCA, glycochenodeoxycholic acid; GDCA, glycodeoxycholic acid; GUDCA, glyco-ursodeoxycholic acid; LCA, litocholic acid; TCA, taurocholic acid; TCDCA, taurochenodeoxycholic acid; TDCA, taurodeoxycholic acid; TUDCA, tauro-ursodeoxycholic acid; UDCA, ursodeoxycholic acid.

Supplementary Table 4. Comparison of the mean (± SD) AUC values of the accumulation of CDCA and GCDCA in the culture medium after various loading periods (0.5, 1, 4, 12 and 24 h) with 10 μM CDCA in SCHH in absence or presence of bosentan. The data presented in Supplementary Figure 3 were used to calculate the AUC values by means of the trapezoidal rule. Conditions were compared to the control condition.

Conditions	AUC of CDCA ± SD (pmol·h)	AUC of GCDCA ± SD (pmol·h)
Control	16589 ± 3370	37361 ± 2612
2.5 μM bosentan	17227 ± 1032	37118 ± 2018
7.5 μM bosentan	18344 ± 2804	37345 ± 1736
25 μM bosentan	19265 ± 1742	38004 ± 2287

AUC, area under the curve; CDCA, chenodeoxycholic acid; GCDCA, glycochenodeoxycholic acid.

Supplementary Table 5. AUC values of GCDCA accumulation in cells and cells+canaliculi after various loading periods (0.5, 1, 4, 12 and 24 h) with 10 μM CDCA and an efflux phase of 15 min in SCHH in absence or presence of bosentan. The data in Supplementary Figure 5 were used to calculate the AUC values by means of the trapezoidal rule. Conditions were compared to the control condition (**p $<$ 0.01 and ***p $<$ 0.001).

	AUC of GCDCA ± SD (pmol·h)	
Conditions	Cells	Cells+canaliculi
Control	1678 ± 217	2420 ± 477
2.5 μM bosentan	1493 ± 16	2349 ± 44
7.5 μM bosentan	1153 ± 160 (***)	1466 ± 148 (**)
25 μM bosentan	853 ± 39 (***)	1284 ± 251 (***)

AUC, area under the curve; GCDCA, glycochenodeoxycholic acid.

References

Oorts M., Baze A., Bachellier P., Heyd B., Zacharias T., Annaert P., and Richert L. (2016). Drug-induced cholestasis risk assessment in sandwich-cultured human hepatocytes. *Toxicology in vitro : an international journal published in association with BIBRA*, 34:179–86.

```
; Bosentan alters endo- and exogenous bile salt disposition in sandwich-
cultured human hepatocytes

; The Journal of Pharmacology and Experimental Therapeutics

; JPET-AR-2021-000695

; Marlies Oorts*, Pieter Van Brantegem*, Neel Deferm, Sagnik Chatterjee,
Erwin Dreesen, Axelle Cooreman, Mathieu Vinken, Lysiane Richert, Pieter
Annaert
; * Shared first authorship

; Control stream used for mechanistic modeling in NONMEM.

$PROBLEM  MODEL BILE ACIDS IVV

$INPUT ID BOS TIME AMT EVID CMT DV

$DATA nonested.csv IGNORE=@

$SUBROUTINE ADVAN13 TOL=9

$MODEL

COMP=(pMED, DEFDOSE, DEFOBS)  ;1 CDCA medium
COMP=(pCELL)                  ;2 CDCA cell
COMP=(mCELL)                  ;3 GCDCA cell
COMP=(mBILE)                  ;4 GCDCA bile
COMP=(mMED)                   ;5 GCDCA medium

$PK
FuCDCAmed = 1        ;fraction unbound medium CDCA
FuGCDCAmed = 1       ;fraction unbound medium GCDCA
FuCDCAcell = 0.654   ;fraction unbound cell CDCA
FuGCDCAcell = 0.805  ;fraction unbound cell GCDCA

KMuptakeCDCA       = THETA(1)*EXP(ETA(1))
VmaxuptakeCDCA     = THETA(2)*EXP(ETA(2))
CLmetCDCA          = THETA(3)*EXP(ETA(3))

; other THETA for each category of BOS
IF (BOS.EQ.0) THEN
TVCLbileGCDCA      = THETA(4)
ENDIF

IF (BOS.EQ.2.5) THEN
TVCLbileGCDCA      = THETA(5)
ENDIF

IF (BOS.EQ.7.5) THEN
TVCLbileGCDCA      = THETA(6)
ENDIF

IF (BOS.EQ.25) THEN
TVCLbileGCDCA      = THETA(7)
```

```
ENDIF

CLbileGCDCA          = TVCLbileGCDCA*EXP(ETA(4))

CLeffGCDCA         = THETA(8)*EXP(ETA(5))
CLupGCDCA          = THETA(9)*EXP(ETA(6))
kflux              = THETA(10)*EXP(ETA(7))

Vcell = 1.37                          ; µL
Vmed = 250                            ; µL

K23 = CLmetCDCA*FuCDCAcell/Vcell
K34 = CLbileGCDCA*FuGCDCAcell/Vcell
K35 = CLeffGCDCA*FuGCDCAcell/Vcell
K53 = CLupGCDCA*FuGCDCAmed/Vmed

$DES

DADT(1) = - (VmaxuptakeCDCA*A(1)/Vmed)/(KMuptakeCDCA + A(1)/Vmed)
DADT(2) =   (VmaxuptakeCDCA*A(1)/Vmed)/(KMuptakeCDCA + A(1)/Vmed) -
K23*A(2)
DADT(3) =   K23*A(2) - K34*A(3) - K35*A(3) + K53*A(5)
DADT(4) =              K34*A(3)                          - kflux*A(4)
DADT(5) =                          K35*A(3) - K53*A(5)  + kflux*A(4)

$ERROR

IF (CMT.EQ.1) THEN
IPRED = A(1)
W = IPRED
IRES = DV - IPRED
IWRES = IRES/W
Y = IPRED *(1+EPS(1))                          ; EPS results in boundary
issues
ENDIF

IF (CMT.EQ.2) THEN
IPRED = A(2)
W = IPRED
IRES = DV - IPRED
IWRES = IRES/W
Y = IPRED *(1+EPS(2)) + EPS(4)
ENDIF

IF (CMT.EQ.3) THEN
IPRED = A(3)
W = IPRED
IRES = DV - IPRED
IWRES = IRES/W
Y = IPRED *(1+EPS(2))
ENDIF

IF (CMT.EQ.4) THEN
IPRED = A(4)
W = IPRED
IRES = DV - IPRED
```

```
IWRES = IRES/W
Y = IPRED *(1+EPS(2)) + EPS(3)
ENDIF

IF (CMT.EQ.5) THEN
IPRED = A(5)
W = IPRED
IRES = DV - IPRED
IWRES = IRES/W
Y = IPRED *(1+EPS(1))
ENDIF

$THETA
(0, 4.05)                ; KMuptakeCDCA
(0, 4.68)                ; VmaxuptakeCDCA
(0, 0.249)               ; CLmetCDCA

(0, 0.0197)              ; CLbileGCDCA0
(0, 0.0133)              ; CLbileGCDCA2.5
(0, 0.014)               ; CLbileGCDCA7.5
(0, 0.0054)              ; CLbileGCDCA25

(0, 0.0462)              ; CLeffGCDCA
(0, 0.216)               ; CLupGCDCA
(0, 0.0125)              ; kflux

$OMEGA ; IIV
0 FIXED
0 FIXED
0 FIXED
0 FIXED
0 FIXED
0 FIXED
0 FIXED

$SIGMA
0.0797             ; prop error
0.299              ; prop error
58.9               ; add error
3.62               ; add error

$ESTIMATION METHOD=1 INTERACTION MAXEVAL=99999 PRINT=1 SIGDIGITS=4 NOABORT
$COV print=E MATRIX=R

$TABLE ID BOS TIME AMT EVID CMT PRED IPRED IRES W IWRES CWRES KMuptakeCDCA
VmaxuptakeCDCA CLmetCDCA CLbileGCDCA CLeffGCDCA NOPRINT ONEHEADER
FILE=Model14_01.txt
```